• U C • FCTUC FACULDADE DE CIÊNCIAS E TECNOLOGIA
UNIVERSIDADE DE COIMBRA

Departamento de Engenharia Electrotécnica e de Computadores

Mestrado Integrado em Engenharia Electrotécnica e de Computadores

Análise do Desempenho da Ligação Ascendente de um Radar Suportado por Fotónica

Marco José Pires Ferreira

Júri:

Presidente: Prof. Doutor Henrique José Almeida da Silva

Vogal: Prof. Doutor Vítor Manuel Mendes da Silva

Orientadora: Prof. Doutora Maria do Carmo Raposo de Medeiros

Coimbra, Setembro de 2018

• U C • FCTUC FACULDADE DE CIÊNCIAS E TECNOLOGIA UNIVERSIDADE DE COIMBRA

Departamento de Engenharia Electrotécnica e de Computadores

Mestrado Integrado em Engenharia Electrotécnica e de Computadores

Uplink Performance Analysis of a Photonics Supported Radar

Marco José Pires Ferreira

Jury:

President: Professor Henrique José Almeida da Silva, PhD

Member: Professor Vítor Manuel Mendes da Silva, PhD

Supervisor: Professor Maria do Carmo Raposo de Medeiros, PhD

Coimbra, September 2018

The work developed in this dissertation was carried out within the framework of the project RETIOT, SAICT-45-2015-03 Project nº 16432, and supported by the IT infrastructure facilities namely the ORCIP Centro-01-0145-FEDER-002141.

Agradecimentos

Em primeiro lugar, gostaria de agradecer à orientadora, Professora Doutora Maria do Carmo Raposo de Medeiros, pela disponibilidade de auxílio, sugestões e aprendizagem, que foram essenciais no desenvolvimento desta dissertação.

Depois é importante agradecer ao Instituto de Telecomunicações – Pólo de Coimbra pelas condições de trabalho disponibilizadas.

E ainda ao grupo de óptica do Instituto de Telecomunicações – Pólo de Coimbra por fornecer modelos Matlab essenciais para o âmbito do trabalho. Nomeadamente, ao Dr. Paulo Alexandre Ferreirinha de Almeida e à Prof Doutora Maria do Carmo Raposo de Medeiros.

Por fim, resta agradecer aos meus pais e à minha irmã, por todo o sacrifício que fizeram para que esta etapa fosse possível.

A todos que me apoiaram, pela sua paciência e dedicação,

Muito Obrigado.

Abstract

Recent years have seen growing pressure on the requirements for remote sensing systems. Radar systems have evolved from their traditional ranging and surveillance applications to a much broader spectrum of applications. They are now evolving toward a new era of multifunctional and multiband frequency operation. This change in perspective is being fueled by the advances made in various fields. These fields range from autonomous-vehicle industry to the healthcare industry. Recently spectrum regulators have released the unlicensed use of the 77 GHz frequency band to be used for vehicular radars, which has encouraged the development of high frequency radar systems.

A need for fast high-resolution imaging is putting pressure on traditional electronic technologies. The lack of electronic systems which have the capacity of directly generating, processing and digitizing stable signals at high frequencies and larger bandwidths, has motivated research worldwide.

Alternatives based on photonic systems have being proposed to overcome the challenges presented by traditional electronic radars. Efforts are now being focused on using the millimeter-wave (MMWave) band with photonic supported systems.

This dissertation begins by exploring the limitations of electronic radar systems. These limitations are presented with tests conducted on a simulation model based on a software defined architecture. Once the drawbacks of the electronic radar are exposed, an introduction to photonic supported radars is presented.

Then, system tests on a simulation model of a photonic supported radar are conducted. Where various systems parameters are tested. With the conducted tests, performance degradation issues of the uplink are evaluated and studied.

Throughout this dissertation, the components and architecture of the photonic and electronic radar are presented and discussed. The presence of phase noise is highlighted since it is one of the main sources of performance degradation in radar systems.

Keywords:

FM-CW Radar, Phase Noise, Electronic Radar, Microwave Photonics, Photonic Radar.

Resumo

Actualmente, os sistemas de sensores remotos estão a entrar numa nova fase. Um aumento na procura de sistemas com capacidades multifuncionais e multibanda está a incentivar investigação e investimento em diversas áreas de indústria. Esta procura está a ser estimulada por avanços tecnológicos em diversas áreas tais como veículos autónomos, aplicações do sector de saúde e em aplicações de casas inteligentes. Os sistemas de radar estão a evoluir para além seu formato tradicional de sistemas de medição de distância e velocidade.

O desempenho de radares de alta definação é dependente de factores tais como o nível de ruído de fase dos osciladores de radio frequência e da largura de banda do sinal radar. Estas limitações podem ser ultrapassadas com a utilização de tecnologias fotónicas.

Esta dissertação começa com o estudo das limitações dos sistemas de radar electrónicos. Essas limitações são apresentadas com testes realizados num modelo de simulação baseado numa arquitetura definida por software. Depois da análise e caracterização das limitações dos radares electrónicos, a solução para algumas destas limitações é apresentada através de sistemas radar suportados por tecnologias fotónicas.

Os últimos capítulos desta dissertação apresentam o modelo de simulação implementado do sistema de radar suportado por fotónica. Vários testes de desempenho são apresentados e discutidos.

Ao longo desta dissertação, os componentes e a arquitetura do radar fotónico e electrónico são apresentados e discutidos. A presença de ruído de fase é destacada, uma vez que é uma das principais origens de erros nos sistemas de radar.

Palavras-Chave:

FM-CW Radar, Ruído de Fase, Radar Electrónico, Fotónica de Microondas, Radar Fotónico.

Table of Contents

List of Figures

List of Tables

List of Acronyms

ASE	Amplified Spontaneous Emission
BP	Band-Pass Filter
CFAR	Constant False Alarm Rate
CW	Continuous Wave
FFT	Fast Fourier Transform
FIR	Finite Impulse Response
FM	Frequency Modulation
FM-CW	Frequency Modulated - Continuous Wave
HRR	High-Resolution Radar
IF	Intermediate Frequency
IQ	In-phase/Quadrature
LFM	Linear Frequency Modulation
LO	Local Oscillator
mmWave	Millimeter-Wave
MZIM	Mach-Zender Intensity-Modulator
MZM	Mach-Zehnder Modulator
O/E	Optic-Electric
OSNR	Optical Signal-to-Noise Ratio
PD	Photodetector
Radar	Radio detection and Ranging
RF	Radio Frequency
RRH	Remote Radio Heads
SNR	Signal-to-Noise Ratio
USRP	Universal Software Radio Peripheral

1 – Introduction

In this chapter, the motivation and scope of the dissertation are presented in Section 1.1. Section 1.2 presents the main objectives. Section 1.3 exposes the outline of this thesis and in Section 1.4 the major contributions of this thesis are summarized.

1.1. Overview and Motivation

Radio detection and ranging (radar[1]) systems have taken on a new meaning since their early days as simple target detection and ranging systems. Nowadays, radar systems have developed a whole new spectrum of capabilities, such as target tracking, target identification and high definition imaging capabilities. Use cases of these modern day radars are present in a broad range of applications, such as military and civilian aircraft tracking, three-dimensional vehicle collision avoidance, earth resource monitoring and many others[1]. These modern radar systems have evolved to systems that conduct estimations with low errors and with inherent high immunity from strong unwanted environmental echos (known as clutter).

Recent years have seen great innovation in radar systems implemented in automotive applications. This innovation has been incited by the advances made in the autonomous vehicle field. Traditional automotive frequency modulated continuous wave (FM-CW) radar systems operate at the 24GHz frequency band. With the recent decision of opening up frequency bands automotive radar applications have migrated to the 77GHz band [2]. The bandwidth present at higher frequencies opens the potential for radar design with higher range resolutions, which are critical for use cases such as autonomous vehicle collision avoidance. The stipulated bandwidth available from 77-81 GHz brings forward bandwidths of up to 4 GHz, while traditional 24GHz systems are limited to a 200 MHz bandwidth. Furthermore, due to higher frequency architectures antenna dimensions are reduced in comparison with 24GHz systems. It is with these advantages in mind that the exploration of higher frequencies is highlighted in this dissertation.

This thesis is focused on FM-CW radar technology. FM-CW radars have already been demonstrated as robust solutions in various fields such as ship navigation, object identification and wind speed and direction estimations. More portable solutions have also been demonstrated in diverse areas, solutions such as fall detection of elderly people[3], breathe detection[4] and in domotic systems. FM-CW radar systems are becoming more portable, more reliable and low-priced.

[1] RADAR is the acronym for RAdio Detection And Ranging, the word radar is presently used as an English noun.

Although FM-CW radars are robust solutions, some drawbacks are still of some concern. Modern electronic FM-CW radars suffer from electromagnetic interference and are susceptible to oscillator noise caused by multiple stage upconversions. The solution to these drawbacks has been proposed by photonic generation of radio frequency (RF) radar signals. In recent years, photonic supported systems have demonstrated the required flexibility to support future radar systems. Paolo Gheldi and his colleagues have conducted the first field demonstration of a coherent photonic radar [5],[6]. Where the proposed system was tested by tracking aircrafts, the estimations were compared to open source data and were proved to be accurate. Photonic technologies also bring forward other advantages such as easy distribution through optical fiber. Due to high frequency atmospheric attenuation, the maximum range of high frequency radars is limited, distributed design schemes present a simple solution to this problem. An example of an optical distributed system for foreign object debris (FOD) detection has been demonstrated[7],[8]. In [8] , field feasibility of the proposed system is evaluated and various advantages are presented. One important advantage of radar based FOD detection systems lies in its robustness against adverse weather conditions. Traditional FOD detections systems are based on infrared cameras and visible light cameras, which suffer from weather conditions such as rain and snow.

Although photonic supported systems have a promising future some performance degradation aspects must be assessed. Some of these performance degradation issues increase noise levels in the radar received signals which consequently originate false-positive targets and degrade the detection quality.

1.2. Objectives

The main objective of this dissertation is the simulation and performance evaluation of a FM-CW photonic supported radar system. This dissertation is focused on the system uplink, i.e. the radar signal generation in the optical domain and its translation to the electrical domain.

The first objective is the understanding of the operating principles of FM-CW radars and the digital signal processing algorithms necessary to treat relevant received signals in order to detect targets. Additionally, system limitations that can be overcome with photonics should be identified.

Software defined approaches are a logical step in modern day radar systems. With this in mind, the starting radar architecture used in this dissertation is based on the universal software defined platforms (USRP) available at the Instituto de Telecomunicações – Pólo de Coimbra. The simulation model should be capable of assessing and characterizing performance limiting factors of electronic FM-CW radar systems. A major drawback of electronic radars is the presence of phase noise generated by electrical oscillators.

This drawback should be studied by emulating a noise carrier with a phase noise profile of a real physical oscillator. The selected noise profile is obtained by measuring the phase noise levels directly from an Ettus X300 USRP. Another use of the simulation model is the verification of system improvements when higher bandwidths are selected. The study on how radar resolution is improved with larger bandwidths is also an objective of this dissertation.

The third objective of this dissertation is the study and implementation of a photonic supported radar system. The simulation model should be able to verify the influence of partially decorrelated mode locked lasers on radar functionality. The analysis of the effect of intensity noise on radar velocity and range estimations should also be verified. The fourth objective is to verify the maximum mode linewidth which maintains stable operation of the photonic radar system.

The final objective of this thesis is the analysis of the combination of all the limiting issues of a photonic supported radar. A global system performance understanding should be presented by calculating figures of merit of the photonic supported radar.

1.3. Dissertation Outline

Following the introductory chapter, chapter 2 presents core concepts on FM-CW radar systems. The radar design equation is presented followed by definitions of range and velocity estimations. Then, key notions on range resolution and velocity resolution are introduced. The final section of chapter 2 presents FM-CW radar drawbacks such as Doppler coupling, nonlinear radar signal generation and finally the notion of phase noise is presented along with its effect on radar systems.

Chapter 3 explores the developed electronic FM-CW radar simulation model. Primarily, the simulated system architecture is discussed then waveform modulation is presented. Then, topics of radar digital signal processing (DSP) are presented and explained. The last section presents the system simulation and conducted test results.

In chapter 4, an introduction to photonics is presented where some relevant advantages of photonic supported systems are exposed. Following the introduction, section 4.2 introduces optical frequency combs. Then, section 4.3 briefly explores optical amplification and noise. Following optical amplification and noise, electrical to optical modulation is presented and discussed. The second to last section introduces the mechanism by which the translation from the optical to electrical domain is conducted. The last section explores the heterodyning method used to generate stable high radio frequency signals.

Chapter 5 explains the simulated photonic supported radar. Where various performance issues are studied. An analysis of how range errors evolve by varying system parameters such as optical signal-to-noise ratio (OSNR) and laser linewidth. The degradation caused by phase decorrelation between laser modes is also discussed.

The final section presents the system performance by means of system figures of merit.

1.4. Contributions

This dissertation was developed in Instituto de Telecomunicações in Coimbra, for the project RETIOT.

The main original contributions of this dissertation are:

-Implementation of a simulation model to study radar performance.

-Radar performance evaluation in function of phase noise.

-Implementation of the uplink of a photonic supported radar.

-Performance evaluation of the uplink of a photonic based radar system as function of the OSNR, laser linewidth and decorrelation between the optical tones.

2 - FM-CW Radar Systems

This chapter explores key properties of FM-CW radar systems, presents the basic theory of remote sensing and discusses key characteristics such as modulation, range, velocity and system functionality. System advantages and disadvantages are also discussed.

2.1. Overview of FM-CW Radars

Continuous-wave (CW) radars are electromagnetic sensors where a known constant frequency/amplitude continuous radio energy wave is transmitted and then partially received from reflecting targets.

Subsequently, received CW radar signals are mixed with a replica of the transmitted signal. This operation enables the extraction of the received signal frequency shift (in comparison with the transmitted signal frequency) which enables the calculation of the target velocity. Due to its continuous nature, CW radars do not include time references. Hence, it is impossible to measure round-trip times of the transmitted signals and consequently target ranges.

Contrary to unmodulated CW radars, FM-CW systems have the ability to extract both range and velocity. By frequency modulating the transmission signal, a valid time reference is created. This characteristic is presented in Figure 2.1, where the received signal is posed against a replica of the transmitted linear frequency modulated (LFM) signal. Here it becomes perceptible that the signals can be mixed for time (range) and frequency (radial velocity) measurements.

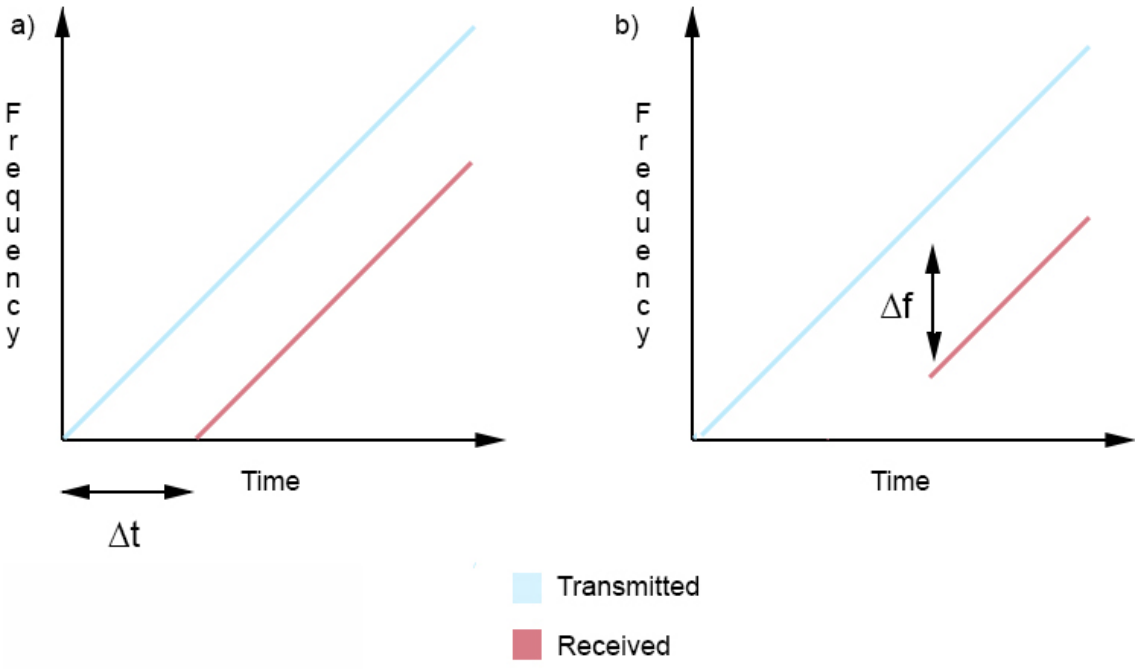

Figure 2.1 - Received and transmitted LFM signals. a) Time shift b) Frequency shift. [9]

2.1.1. Radar Equation

The radar equation plays an important role in radar design. It equates range as a function of system characteristics and physical processes.

Sensing systems usually make use of directional antennas that direct energy into a certain volume of space, therefore the peak power density at a distance R from a radar is defined as [9]

$$P_D = \frac{P_t\, G}{4\pi R^2} \tag{1}$$

where P_t , is the peak transmitted power and the G parameter characterizes the directional antenna gain and is composed of the following fraction

$$G = \frac{4\pi A_e}{\lambda^2} \tag{2}$$

λ denotes the radar signal wavelength and A_e is the effective aperture of the directional antenna. A_e relates to the antenna´s physical aperture A by means of ρ, the aperture efficiency.

$$\begin{gathered} A_e = \rho A \\ 0 \leq \rho \leq 1 \end{gathered} \tag{3}$$

Electromagnetic sensors depend on target reflections, implicating that reflected energy must be accounted for in the radar equation. Hence, the radar cross section is introduced.

An object exposed to an electromagnetic wave disperses energy in all directions, a phenomenon known as scattering, the amount of scattered energy is proportional to the target size, physical shape, orientation and material of the object. All of these characteristics are combined to form the radar cross section (*RCS*), denoted by σ.

$$\sigma = \lim_{R\to\infty} 4\pi R^2 \frac{|E_s|^2}{|E_0|^2} \tag{4}$$

The *RCS* is the ratio between the electric field strength, E_0 , and the scattered wave electric field strength, E_s , of the incident wave. The radar equation may finally be written as

$$P_r = \frac{P_t\, G}{4\pi R^2} \times \frac{\sigma}{4\pi R^2} \times A_e \tag{5}$$

P_r is the portion of reflected power obtained by the receiver antenna with an aperture of A_e, the denominator of the second factor to the right accounts for divergence of the echo(reflected) signal on its return path after being reflected on a target with RCS equal to σ. Suppose that the radar has a minimum detectable signal power, S_{min}, another variable is introduced, R_{max}, which represents the maximum range and is defined by the following

$$R_{max} = \left(\frac{P_t\, G^2 \lambda^2 \sigma}{(4\pi)^3 S_{min}} \right)^{1/4} \tag{6}$$

According to equation 6, to double the maximum range, the peak transmitted power, P_t , must be increased sixteen times or A_e , the effective aperture, must be increased four times. The preceding equation neglects variables such as clutter, noise and system losses.

2.1.2. Range Estimation

FM-CW radars extract range measurements by means of heterodyning (mixing) the transmitted signal with the received signal. After heterodyning an intermediate frequency is obtained, typically known as the beat frequency, fb, or the *dechirped* signal frequency.

$$fb = freceived - ftransmitted \tag{7}$$

By employing geometric relations, it is possible to obtain the expression for the time and frequency shifts. These relations are depicted in Figure 2.2 a).
Denoted as the sweep slope, α, the relationship between radar bandwidth B and radar sweep time period T is presented.

$$\alpha = \frac{B}{T} \tag{8}$$

The time delay, Δt , of the received signal is defined as

$$\Delta t = \frac{2R}{c} \tag{9}$$

where R expresses target range and c the speed of light in vacuum.
By multiplying the sweep slope with the time delay it is possible to define the beat frequency in function of range

$$fb = \alpha \times \frac{2R}{c} \tag{10}$$

the division of the right side of the equation quantifies the time delay caused by the round-trip time of the transmitted signal.

2.1.3. Velocity Estimation

The Doppler frequency shift is used to extract radial velocity as well as to distinguish moving targets from stationary objects, such as clutter (unwanted echoes).

This frequency shift is obtained by verifying the frequency deviation of an echo signal with respect to the transmitted signal, presented in Figure 2.2 b). The received frequency of targets that are moving in the direction of a stationary radar, will be higher than the emitted frequency, while the received frequency of a target moving away from a stationary radar will be lower than the transmitted frequency. The Doppler shift can be described as

$$f_d = \frac{2v_r}{\lambda} = \frac{2v\,cos\theta}{\lambda} = \frac{2v_r f_0}{c} \tag{11}$$

Where $v_r = v\,cos\theta$ represents the relative velocity of a target for a stationary radar, v expresses the absolute velocity of the target, λ is the radar signal wavelength, f_0 is the center frequency of the transmitted signal. θ characterizes the angle between the target direction and the radar beam.

It should be noted that with the use of simple sawtooth waveforms, a coupling error is present in range estimations. Figure 2.2 b) demonstrates the origin of this error, the doppler frequency and beat frequency are formed along the same dimension[2].

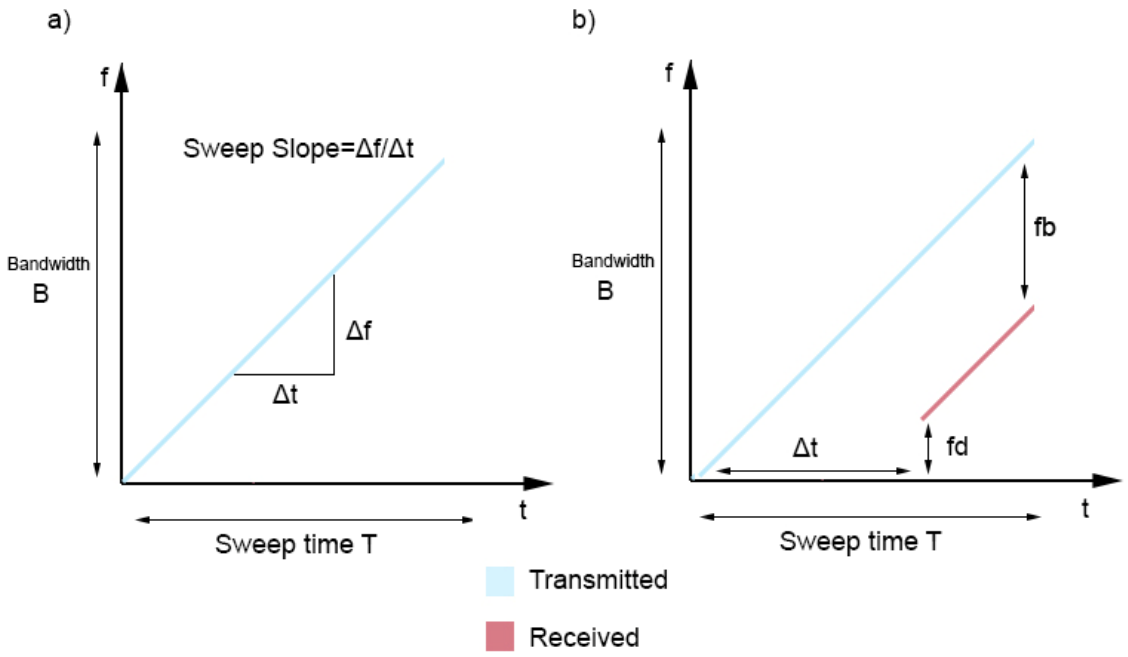

Figure 2.2 - Received and transmitted LFM signals. a) LFM Sweep slope b) Frequency and time shift.

2.2. Radar Resolution

Radar resolution is a radar´s capability to completely distinguish targets that are relatively close to each other or that have similar velocities.

This ability is affected directly by LFM nonlinearity [10] and by phase noise introduced by voltage-controlled oscillators (VCO)[11].

In contrast, the compression gain (pulse compression), is a characteristic which improves radar resolution and radar performance, FM-CW systems are inherently pulse compressed, this characteristic is observed by the reduced bandwidth of the dechirped (heterodyned) signal in comparison with the cross-correlation of a simple radar pulse[12].

[2]Further discussion of this topic is covered in section 2.3.1

2.2.1. Range Resolution

Range resolution, denoted as ΔR, is a radar metric which quantifies the distance between two or more targets. Consequently, range resolution can be defined as the minimum unambiguous distance to which distinction between targets is possible. This metric plays an important role in high range resolution (HRR) sensors. By minimizing ΔR , higher resolution is obtained.

By considering two targets at unambiguous ranges R_1 and R_2 ,with corresponding time delays Δt_1 and Δt_2, range resolution can be expressed as

$$\Delta R = R_2 - R_1 = c\frac{\Delta t_2 - \Delta t_1}{2} \tag{12}$$

the inverse of the unambiguous time interval, ($\Delta t_2 - \Delta t_1$) is equal to the radar bandwidth B. Range resolution takes the final form of

$$\Delta R = \frac{c}{2B} \tag{13}$$

It should be noted that to achieve improved resolution, the radar signal bandwidth must be increased. Therefore, demonstrating the importance of the radar bandwidth in high resolution radar design.

2.2.2. Velocity Resolution

Similar to range resolution, velocity resolution $\Delta \mathrm{v}$, is the minimal radial velocity difference between two targets travelling at the same range before a radar can detect two reflections. It can be described as

$$\Delta \mathrm{v} = \frac{c\,\Delta_{f_d}}{2f_0} \tag{14}$$

With f_0 denoting the central frequency, c the speed of light in vacuum and Δ_{f_d} the unambiguous difference of doppler frequencies between two moving targets.

2.3. Drawbacks of FM-CW Radar

Although FM-CW radars present various advantages, such as a heterodyne based architecture, both range and velocity measurements, system stability and short-range capabilities. Some design

considerations must be accounted for. Especially, nonlinear sweep frequencies and phase noise sensitivity. These are the two greatest performance limiting characteristics of FM-CW sensing systems.

Phase noise in FM-CW radar systems is a central topic of this dissertation. Therefore, a more in-depth discussion is presented in section 2.3.3.

2.3.1. Doppler Coupling

A known issue associated with LFM signals is the range Doppler coupling effect. As previously mentioned, the beat frequency corresponds to target range. Hence, range measurements are dependent on valid beat frequency estimations. In the presence of doppler shifts, the beat frequency is biased, resulting in range estimations errors.[13]

Doppler coupling becomes more prominent when sweep times T are longer, which for certain applications may not suffice, since longer sweep times correspond to lower sampling frequencies.

This problem can be resolved by designing a radar system that implements an alternating frequency modulated waveform i.e. triangular signal.

Let it be noted that subsequent simulations in this dissertation make use of simple LFM sawtooth waveforms, prone to doppler coupling. All doppler coupling errors are accounted for by means of range offset calculation[14].

$$\text{Range Offset} = \frac{c \times fd}{2 \times \alpha} \tag{15}$$

Where c is the speed of light in vacuum, fd ,the doppler frequency shift and α the radar sweep slope.

2.3.2. Nonlinear Sweep Frequency

Nonlinear LFM modulation is another issue that influences system performance. LFM waveforms have rectangular power spectrums that originate range sidelobes in the time domain. This propriety has been assessed to the level of nonlinearity of sweep signals. The effect of nonlinearity has been demonstrated to cause significant increases in range sidelobes [15]. Therefore, nonlinearity widens the dechirped signal bandwidth, deteriorates range resolution and aggravates system errors.

2.3.3. Phase Noise

Electrical oscillators are widely used in communication and radar systems. In frequency modulated radars, they are tasked with linear frequency modulating the carrier signal,

upconversion and consequently downconversion of transmission and receive signals. However, the presence of phase noise deteriorates radar system performance.

An ideal oscillator would produce a pure sine wave, which in the frequency domain would be presented as a signal pair of Dirac delta functions. All the power of an ideal sine wave is concentrated at the defined oscillation frequency. In the case of real oscillators, the power of the signal is spread to adjacent frequencies due to the phase noise components. This phenomenon creates noise sidebands.

The characterization of phase noise of a simple carrier sine wave signal can be expressed as follows [16]:

Assuming a noise-free signal, *x(t),* with an amplitude *A* and an operating frequency f_0.

$$\mathrm{x(t)} = A\cos(2\pi f_0 t) \tag{16}$$

The phase noise, $\varphi(t)$, a stochastic process, is added to the sine wave as follows

$$\mathrm{x(t)} = A\cos(2\pi f_0 t + \varphi(t)) \tag{17}$$

The addition of this component creates phase noise sidebands visible in the frequency domain and characterized by $\mathcal{L}(f)$.

The signal´s phase noise, $\mathcal{L}(f)$, is represented as the fraction between the noise sideband power and the carrier power at a certain frequency offset from the carrier

$$\mathcal{L}(f) = \left[\frac{Psideband(f_o+f,1Hz)}{P_{carrier}}\right] \tag{18}$$

where $P_{sideband}(f_o + f, 1Hz)$ is the single sideband power at a frequency offset of f from the carrier, in a bandwidth of 1Hz, and $P_{carrier}$ is the carrier power.

In general, phase noise, $\mathcal{L}(f)$, follows a piece-wise linear function. An example of the piece-wise linear function of phase noise is present in Figure 2.3 a). Figure 2.3 b) depicts the experimental measurement conducted of the oscillator present in the USRP, Ettus X300. The measurement of the noise profile was conducted at an operating frequency of 4 GHz.

The electronic radar model simulation in the following chapter operates with the measured noise profile of the USRP present in Figure 2.3 b).

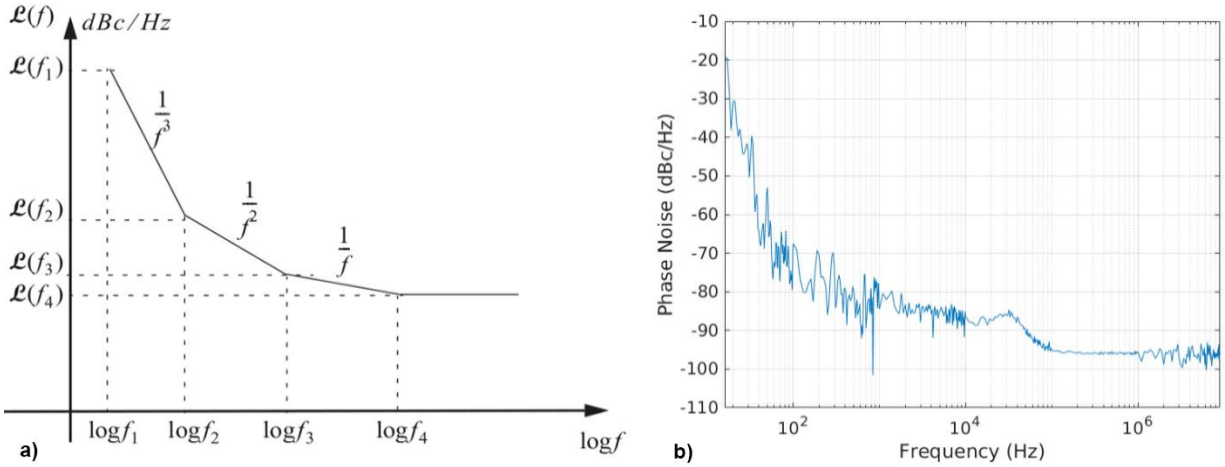

Figure 2.3 - Phase noise profiles. a) Example of phase noise profile [9]. b) Phase noise profile of the USRP Ettus X300 measured in the laboratory.

Phase noise limits the radar capability to detect slow moving objects with relatively small *RCS*. This masking effect is illustrated in Figure 2.4.

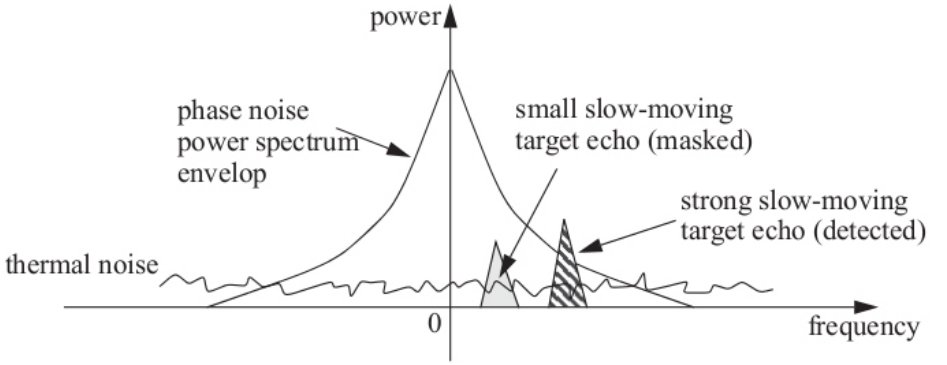

Figure 2.4 - Phase noise masking effect. [9]

3 - Electronic FM-CW Radar Model

In this chapter, the model of FM-CW Radar system is implemented using Matlab. The model is based on the architecture of the Ettus USRP X300. System operational parameters are specified. Schematics of relevant system components and simulation concretization is discussed. DSP based performance metrics are also presented, laying the groundwork for system analysis of a photonic based FM-CW radar in subsequent chapters.

3.1. System Architecture

The architecture design of the software-defined FM-CW radar system is illustrated in Figure 3.1.

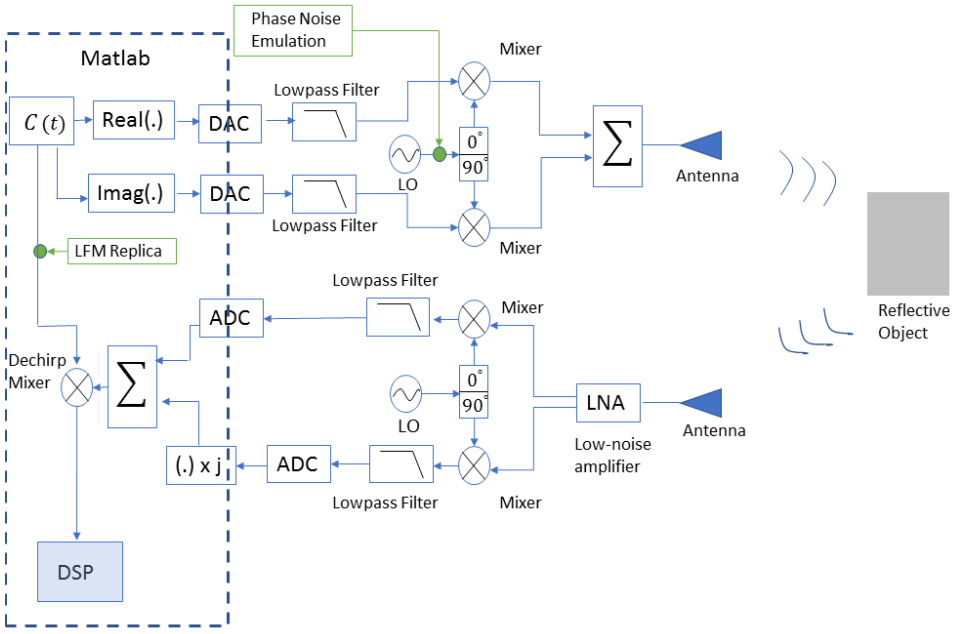

Figure 3.1 - Electronic FM-CW architecture

In the Radar uplink a digital baseband radar signal, $C(t)$, is generated using Matlab. $C(t)$, is a complex signal with real components (in phase) and imaginary components (quadrature). This signal is consequently downloaded to the USRP.

At the USRP, the digital samples of the $C(t)$ signal are converted to the analog domain by means of digital-to-analog converters (DAC). This conversion is followed by low pass filtering that removes high frequency components generated by the conversion process. Once the signal is filtered, two transmission paths are upconverted to the frequency of the local oscillator (LO). The

LO is a hardware functional block that is characterized by its frequency, power, phase noise and frequency drift. The simulation model implemented includes phase noise.

After the upconversion process the phase and quadrature (IQ) components are combined and radiated through an antenna. After reflection on a target, an echo signal is received. A low noise amplification (LNA) of the signal is executed, followed by the downconversion process. The downconversion process is considered ideal since phase noise of the receiver´s LO is neglected. It is relevant to mention, that in the case of upconversion/downconversion conducted by a single LO, the phase noise is correlated between transmitted and received signals. This propriety can result in better system performance.

After downconversion the analog IQ components are combined and converted back to digital signals (ADC).

The next step in the radar system, which is realized by signal processing using Matlab, consists in digitally heterodyning the received signal with a replica of the transmitted signal. This operation produces the dechirped signal which is then digitally processed for the extraction of range/velocity estimates.

3.2. Equivalent Baseband Radar Signal

A LFM radar RF signal, defined during a sweep time period T, and with bandwidth B, can be represented as

$$x(t) = Acos(2\pi f_o t + \pi\alpha t^2) \tag{19}$$

where A is the amplitude, f_o, the RF frequency, α is the LFM slope defined as $\alpha = \pm\frac{B}{T}$, + if the LFM signal has a positive slope (up-chirp) and – if the LFM slope is negative (down-chirp). The phase of the LFM signal is

$$\emptyset(t) = \pi\alpha t^2 \tag{20}$$

The instantaneous frequency deviation from f_o, is calculated as

$$f_i(t) = \frac{1}{2\pi}\frac{\emptyset(t)}{dt} = \alpha t = \pm\frac{B}{T} \tag{21}$$

from equation (19), $x(t)$, can be written as

$$x(t) = A[cos(\pi\alpha t^2)\cos(2\pi f_o t) - sin(\pi\alpha t^2)sin(2\pi f_o t)] \tag{22}$$

or in terms of the component in phase, $C_I(t)$, and the component in quadrature, $C_Q(t)$,of the complex envelope, $C(t)$, of the LFM signal

$$C(t) = e^{j\pi\alpha t^2} \tag{23}$$

The component in phase $C_I(t)$, and the component in quadrature $C_Q(t)$are respectively:

$$\begin{aligned} C_I(t) &= cos(\pi\alpha t^2) \\ C_Q(t) &= sin(\pi\alpha t^2) \end{aligned} \tag{24}$$

The equivalent baseband digital radar signal $C(t)$ is calculated in Matlab using the function *phased.FMCWWaveform*. Figure 3.2 below illustrates the $C_I(t)$ and $C_Q(t)$ components of the baseband equivalent LFM signal.

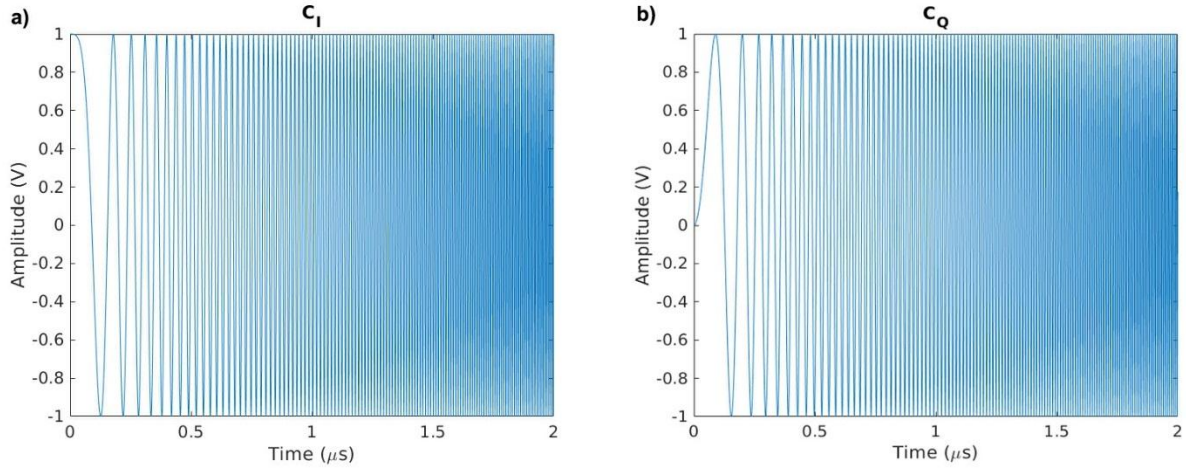

Figure 3.2 - Radar Baseband Signal. a) In phase component. b) In quadrature component.

Figure 3.3 illustrates a spectrogram of a typical LFM signal with $\alpha = 6.25e13\ s^{-2}$. The spectrogram is a representation of the frequency components of the signal as they vary with time.

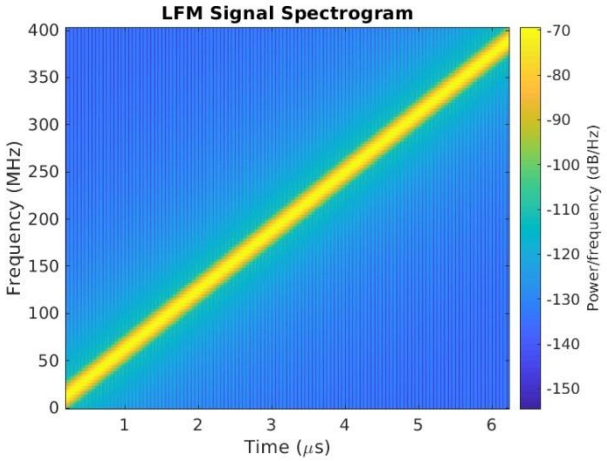

Figure 3.3 - Typical LFM signal spectrogram. The vertical axis represents the frequency variation and the horizontal axis represents the time axis. The frequency components are computed with a FFT.

The spectrum of the signal is illustrated in Figure 3.4. Since it is not a real signal it does not have Hermitan symmetry.

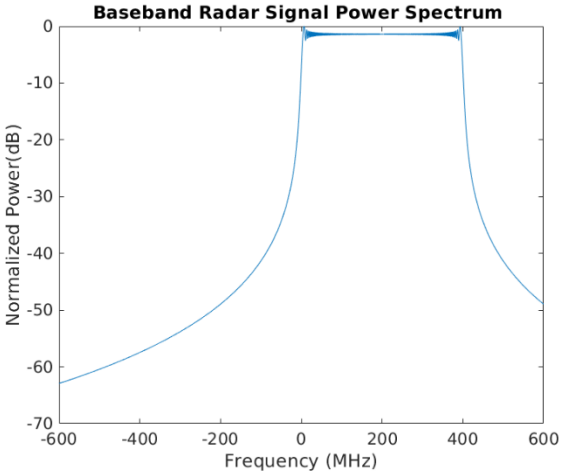

Figure 3.4 - LFM baseband signal power spectrum.

3.3. Phase Noise Model

The simulation model of the LO phase noise follows the algorithm presented in [17], which is illustrated in Figure 3.5. And was implemented with the Matlab method *comm.PhaseNoise*.

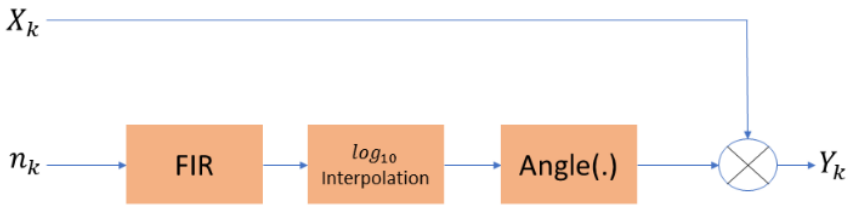

Figure 3.5 - Phase noise emulation model. [17]

The phase noise induced output signal,Y_k, is defined by

$$Y_k = X_k e^{j\varphi_k} \tag{25}$$

where X_k is a noiseless carrier input signal and φ_k is the phase noise profile, that can be adjusted according to the measured phase noise of a real oscillator.

The phase noise is initial generated by filtering a Gaussian noise signal denoted by n_k. Once the Gaussian noise is filtered with a finite impulse response (FIR) filter, the noise spectrum mask sequence is logarithmically interpolated across the desired frequency offsets, originating the final noise skirt. The phase noise is then applied to the IQ carrier by mixing the input signal with the generated phase noise sequence.

After the LO phase noise generation, the noise induced in phase and quadrature components are mixed with the modulated, $C(t)$,signal and combined to form a RF signal. The RF signal is then radiated through an antenna.

3.3.1. Dechirped Signal SNR

After the mixing process, of the received echo with the transmitted LFM waveform, the dechirped signal is digitally low pass filtered.

Since the LFM waveform has a *sinc* spectrum the dechirped signal contains sidelobes which must be mitigated by applying window functions.

The SNR of the dechirped signal is estimated by multiplying the dechirped time series with an Hanning window function before calculating the fast fourier transform (FFT) [18]. Since the window function attenuates the signal, the overall power of the signal is then readjusted.

3.4. Radar Digital Signal Processing

To assess radar performance two digital signal processing (DSP) techniques were considered. Namely, the Root MUSIC (MUltiple SIgnal Classification) algorithm and The Constant False Alarm Rate (CFAR) algorithm.

3.4.1. Radar Data Cube

Usually, radar data is organized in a cube. This cube is illustrated in Figure 3.6.

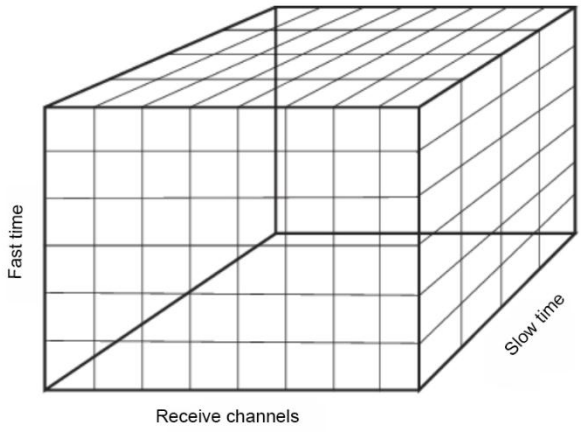

Figure 3.6 - Radar data cube.

The first dimension of the radar cube is denoted as the fast time dimension which contains complex-valued samples grouped in range labelled bins. These range bins are computed by sampling the radar data cube along the vertical axis, for a complete range map of all targets at different velocities, all of the radar sweeps (slow time dimension) are computed i.e. range computation of all column vectors of the data cube. The designation of fast time originates from the fact that the sampling frequency along this dimension is the highest of the overall system. The selection of this sampling frequency depends on system requirements. Larger fast time sampling frequencies originate range bins with more samples and consequently higher range precision.

The second dimension of the radar cube, denoted as the slow time dimension, contains complex-valued samples from different sweeps corresponding to the same range. FFTs along this dimension are conducted at the lowest sampling frequency of the overall system. For a complete velocity map for targets at different ranges, all row vectors are computed. Typically, if LFM waveforms are emitted back-to-back i.e. sawtooth wave, the slow time sampling frequency is equal to the inverse of the chirp sweep time period T.

The third dimension of the radar data cube is present when several receive channels are implemented i.e. phased array systems. This dimension becomes more relevant in the next chapter where Remote Radio Heads (RRH) used in photonic based radars are discussed. System simulations in this dissertation were conducted with only one receive channel.

3.4.2. Root MUSIC Algorithm

The Root MUSIC Algorithm explores the orthogonality between the desired dechirped signal and embedded noise[19]. The range and velocity estimation process is exemplified in Figure 3.7.

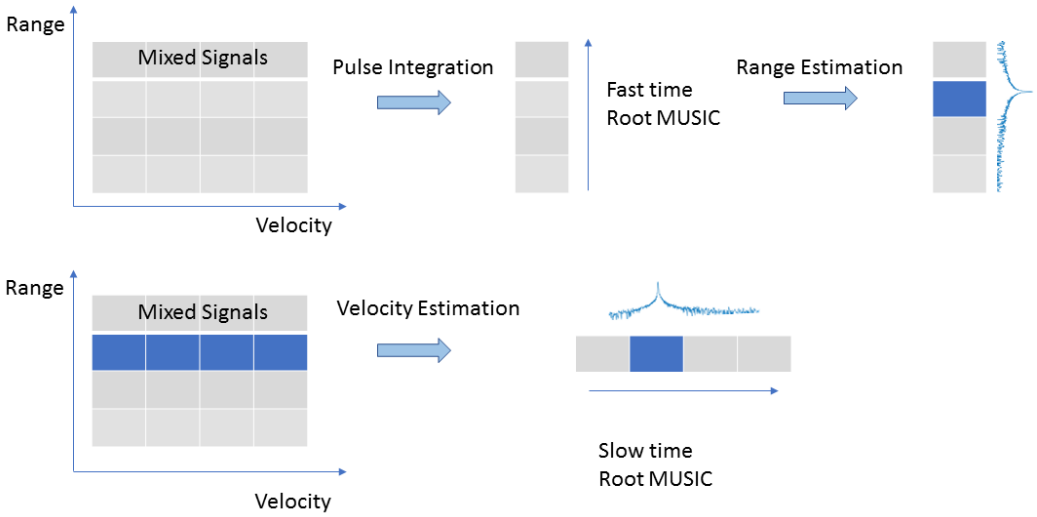

Figure 3.7 - Root MUSIC Algorithm. [19]

The algorithm begins with coherent sweep integration which reduces the two-dimension range-doppler map to one dimension. This integration is administrated along the range samples and can be viewed as the sum of range samples along all system sweeps. The resultant one-dimension range vector is then swept with the fast time Root MUSIC algorithm along all the range bins. Resulting in a final range estimate.

The Root MUSIC algorithm is run again on the original range-doppler matrix, fixed at the previous range estimate, with the slow time sampling frequency. This operation is conducted along all the system´s sweeps and originates the velocity estimate.

Although the Root MUSIC algorithm performed well in conducted simulations, it suffers from a major drawback. The algorithm needs information on how many targets are present beforehand.

3.4.3. Constant False Alarm Rate Algorithm

The Constant False Alarm Rate (CFAR) algorithm is more widely used and does not suffer from the same problem as the Root MUSIC algorithm regarding the detection of multi-targets. It estimates range and velocity by analyzing noise levels in adjacent samples. Thus, providing an adaptive threshold and mulit-target capabilities. Figure 3.8 illustrates the CFAR algorithm functionality.

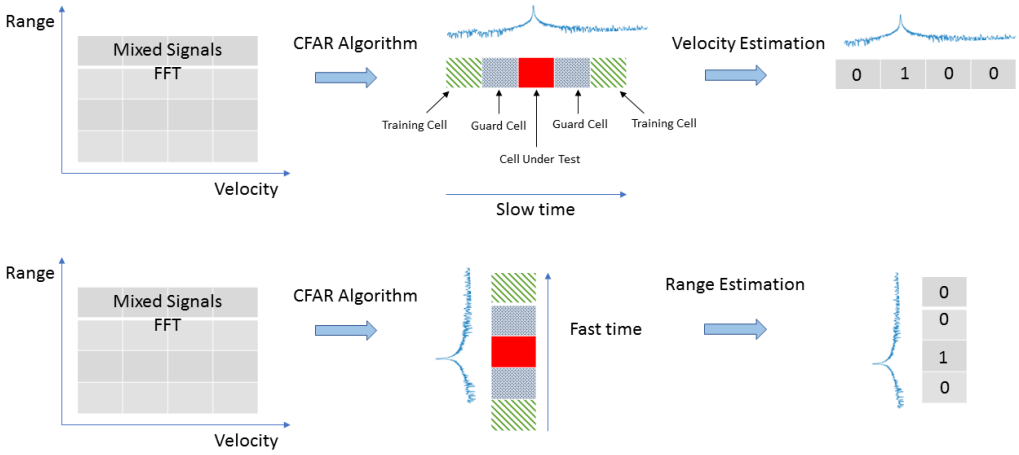

Figure 3.8 - CFAR Algorithm.

3.5. System Simulation

To assess system performance the following metrics for range and velocity errors were applied.

$$Range\ error = |Test\ Range - Range\ Estimate| \quad (m)$$
$$Velocity\ error = |Test\ Velocity - Velocity\ Estimate| \quad (ms^{-1}) \tag{26}$$

The range and velocity estimates are obtained from the Root MUSIC computation while the test velocity and range values are direct inputs of the simulation model.

3.5.1. Radar System Parameters

System simulations were conducted with the parameters present in Table 1. In the following simulations, some of these parameters will be changed and will be specified, the unspecified parameters remain the same.

	Parameter and description	**Value**	**Units**
Physical Parameters	c_o Light speed in vacuum	2.99792458×10^8	ms^{-1}
Radar Parameters	f_o Operation Frequency	4	GHz
	λ_o Operation Wavelength	$\frac{c_o}{f_o}$	m
	B LFM Bandwidth	200	MHz
	T LFM Time Period	10	μs
	α Sweep Slope	$\frac{B}{T}$	s^{-2}

	T Sweep Interval	10×10^{-6}	s
	ΔR Range Resolution	0.75	m
	Δv Velocity Resolution	0.09975	ms^{-1}
	R_{max} Maximum Target Range	30	m
	V_{max} Maximum Target Speed	10	ms^{-1}
	P Average Transmitted Power	0.5	w
Other Parameters	f_s Sample Rate	$2 \times B$	Hz
	N Range FFT Length	2048	-
	L Velocity FFT Length	2048	-
	N_{sweep} Number of Sweeps	2048	-
	σ Target Mean RCS	1	m^2

Table 1 – Electronic radar systems parameters

All system simulations conducted throughout this dissertation assume a free space propagation model. The transmitted and received signals are scaled by the path loss l.

$$l = \frac{(4\pi R)^2}{{\lambda_o}^2} \tag{27}$$

where λ_o is the operational wavelength and R is the target range. This equation assumes that the target is in the far field of the transmitting antenna.

The incident wave on the target is also scaled by the parameter G, which accounts for the portion of energy lost on reflection.

$$G = \sqrt{\frac{4\pi\sigma}{{\lambda_o}^2}} \tag{28}$$

Where σ is the target mean RCS, λ_o is the operational wavelength and R is the target range.

Disturbances caused by components such as mixers and amplifiers were not accounted for.

3.5.2. Radar System Performance

The first step of the electronic radar performance evaluation was conducted with a noiseless carrier and consisted in verifying the effects of compression gain and radar resolution on the developed system.

The study of radar resolution and its impact on radar performance is illustrated in Figure 3.9 and Figure 3.10. Figure 3.9 depicts system performance when the radar bandwidth,B, is equal to

200 MHz. Figure 3.10 depicts the system performance when the bandwidth, B, is equal to 50 MHz. As previously stated, radar resolution is improved with higher bandwidths. This characteristic is seen in Figure 3.9 a), which is the range dechirped signal. By observing Figure 3.9 a), it possible to verify that the system recognizes one target that is not masked by noise.

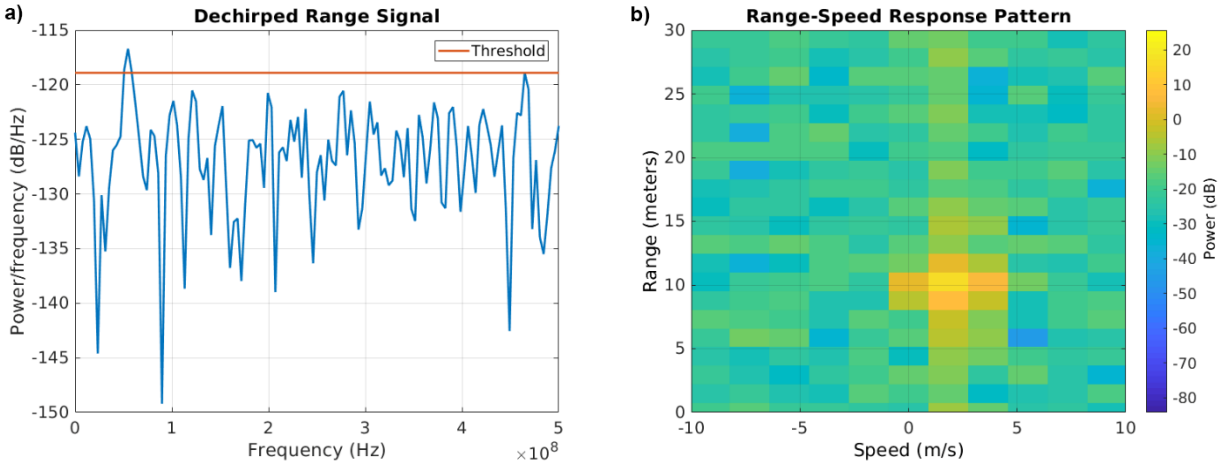

Figure 3.9 - System Performance with B = 200MHz. a) Dechirped range signal. b) Range-speed response pattern.

Contrary to Figure 3.9, Figure 3.10 illustrates the reduced power of the received dechirped signal, which causes false-positive targets along the range dimension and degrades systems performance, visible in Figure 3.10 b). This characteristic is caused by the relationship between the beat signal SNR and the radar resolution.

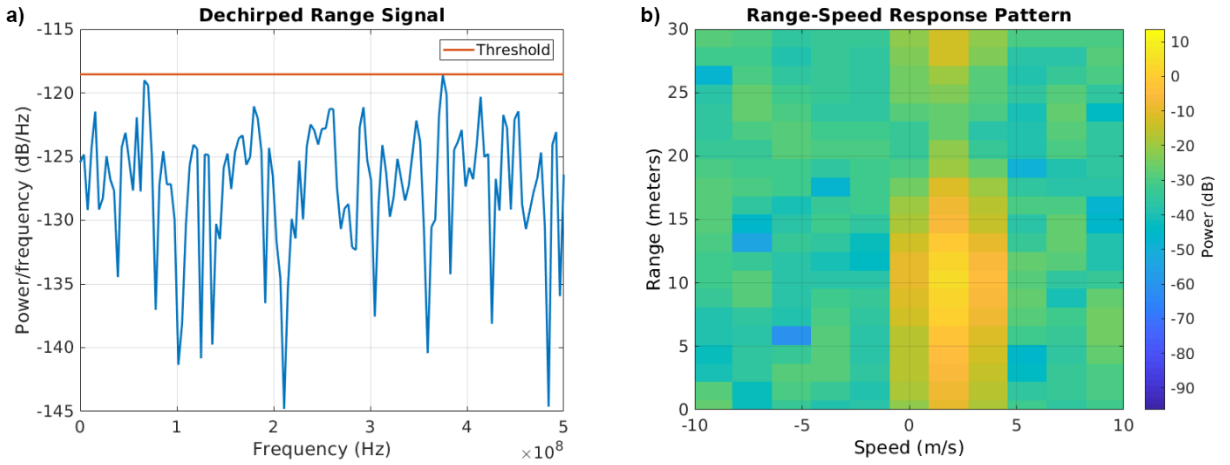

Figure 3.10 - System Performance with B = 50MHz. a) Dechirped range signal. b) Range-speed response pattern.

The compression gain increases the dechirped signal SNR and the radar resolution. It has an important role in high resolution radar design and can be optimized with photonic based radars,

which is discussed in the following chapters. It consists in minimizing the bandwidth of the dechirped signal while maintaining a high SNR. FM-CW radars are inherently pulse compressed, the compression ratio, $\frac{T}{T'}$, defined by the ratio between the LFM time period before compression, T , with the LFM time period after heterodyning, T'. Since the LFM waveform has a rectangular power spectrum its corresponding time period after heterodyning is approximated by

$$T' \approx \frac{1}{B} \tag{29}$$

where B is the LFM bandwidth.

In the developed system, the compression ratio is reduced when B is equal to $50\ \mathrm{M}Hz$. The power of a compressed pulse is defined by

$$P' = P \times \frac{T}{T'} \tag{30}$$

where P' is the compressed pulse power and P is the power before compression.

Table 2 presents additional parameters used in the study of compression gain present in Figure 3.9 and Figure 3.10.

Parameters	**Figure 3.9**	**Figure 3.10**	**Units**
Target Range	10	10	m
Target Velocity	2	2	ms^{-1}
ΔR Range Resolution	0.75	3	m
B LFM Bandwidth	200	50	MHz
$\frac{T}{T'}$ Compression Ratio	2000	500	-
Receive Gain	0	0	dB

Table 2 - Additional electronic radar parameters

Following the evaluation of the influence of pulse compression, an evaluation of how phase noise influences range estimates was conducted. To do so, a stationary target location was incremented in an interval of 0 to 1 meters. This interval was selected since phase noise affects the measurement resolution, corresponding to low beat frequencies, which are masked by the noise present in the radar carrier. Figure 3.11 depicts the tests conducted with the Ettus X300 noisy carrier and an ideal carrier.

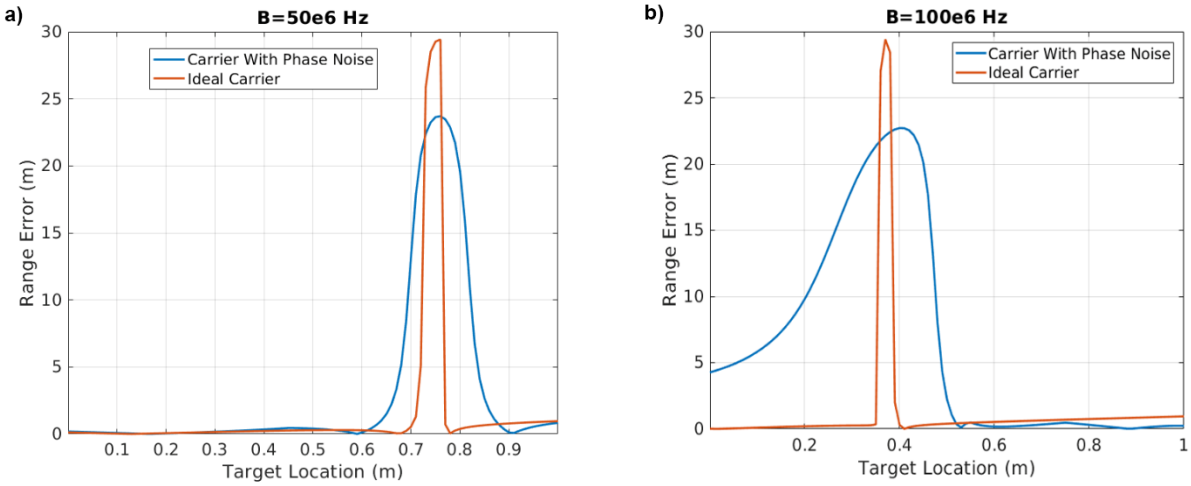

Figure 3.11 - Range error in function of target location. a) Carriers with B=50MHz. b) Carriers with B=100MHz.

The influence of phase noise decreases the measurement resolution, this happens because the beat frequency is masked by the phase noise power spectrum. Although the ideal carrier should not present errors when targets are closer and slower, there is still a relatively high error when the carrier is ideal. Contrary to the carrier with phase noise, these errors are restricted to a smaller range of target locations.

4 - Photonic Supported Systems

This chapter introduces the use of photonic technologies for the development of high definition radars. Key photonic technologies such as high frequency RF signal generation, optical signal modulation, optical to electrical conversion and the optical heterodyning method are discussed.

4.1. Overview of Photonic Technologies

Traditional microwave components suffer from some performance limiting issues. Examples of such drawbacks are noisy analogue up- and downconversions, limited bandwidths and high noise levels at higher frequencies [20],[1],[21]. These disadvantages, in the case of radar systems, deteriorate system performance by limiting resolution, masking targets and increasing processing time.

Microwave photonic technologies have been proposed as a solution for the previously stated drawbacks[22]. These technologies allow extremely stable generation of RF waveforms with ultrawide bandwidths[23],[24]. Other advantages such as electromagnetic interference immunity, easy distribution of RF signals through optical fibers, high tunability and the capability of RRH distribution can be achieved with photonic based systems. It is with these advantages in mind that a photonic based system model is studied in the subsequent sections.

4.2. Optical Frequency Comb

An optical frequency comb is a number of precisely spaced and equidistant optical carriers that share a strong phase correlation. Optical frequency combs are generated from a single device or subsystem. Different techniques have been developed to generate optical correlated tones including mode-locked lasers (MLL) [25],laser gain switching [26] and external modulation of single optical source modulated by a Mach-Zehnder modulator [27]. In this dissertation a MLL is considered.

The key parameters of the laser combs considered in the context of this dissertation are: optical spectral linewidth, $\Delta\lambda$, and optical signal to noise ratio (OSNR). Figure 4.1 illustrates schematically these quantities. The spectral linewidth of a laser tone is typically the full width at half-maximum, FWHM, i.e. 3 dB above the maximum power. OSNR, in this dissertation, is defined as a measure of the ratio of power to noise power floor level.

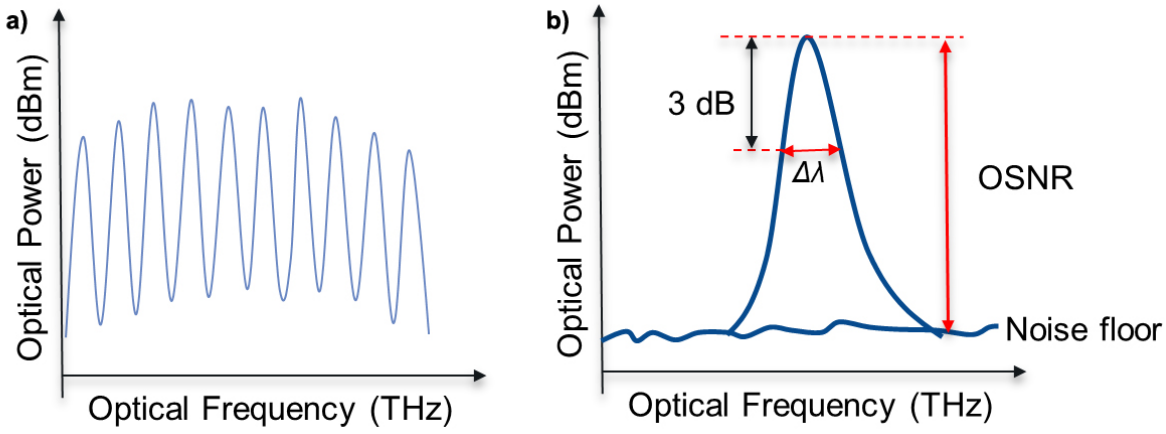

Figure 4.1 - a) Illustrative optical spectrum of a MLL laser. b) Single mode OSNR and linewidth definition.

4.3. Optical Amplification and Noise

Optical amplifiers are used to boost signals and to compensate for the system losses. Optical amplification also adds noise to the system. The noise is caused by the spontaneous emission generated photons in the amplifier. The power spectral density of the amplified spontaneous emission (ASE) is nearly constant (white noise) and can be expressed as[28]:

$$S_{ASE}(v) = (G-1)n_{sp}hv \tag{31}$$

where G is the gain of the optical amplifier, n_{sp} is the spontaneous emission inversion factor, $h = 6.626 \times 10^{-34}$J is the Plank constant and v is the optical frequency.

4.4. Electrical to Optical Modulation

Electrical to Optical (E/O) modulation can be accomplished by external modulation of an optical carrier by means of a lithium niobate (LiNbO3) Mach-Zender (MZM) intensity-modulator. This modulation scheme has proved to be reliable due to its frequency range and stability. In this dissertation, a single-drive Mach-Zender is implemented for the LFM optical waveform modulation.

A MZIM is composed of two LiNbO3 identical waveguides which form the two arms of the intensity modulator. The refractive index of materials such as LiNbO3 is changed by applying external voltages. These external voltages change the phase of the input optical field. Thus, each arm may be considered as an electro-optic phase modulator (EOPM). By phase modulating, a phase delay of the optical field is induced. In the case of a single-drive MZM, only one arm is phase modulated with an exterior electrical driving signal. The two optical fields at the output of

each arm are then coherently added together by a coupler and interfere with each other either constructively or destructively. Figure 4.2 depicts the MZIM schematic.

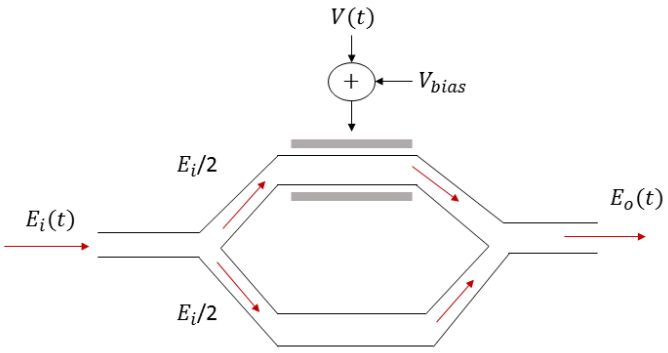

Figure 4.2 - Schematic of the Mach-Zender intensity-modulator. [7]

Where E_i is the input optical field which is split between the two arms, $V(t)$ is the driving voltage, V_{bias} is a DC bias voltage coupled with the driving signal and E_o is the output optical field.

The phase delay, φ, introduced by the driving arm corresponding to a particular RF electrical signal is defined by

$$\varphi(t) = \frac{(V(t) + V_{bias})}{V_\pi} \tag{32}$$

V_π is the driving voltage required to create a π phase shift on the light wave carrier and has typical values within a range of 3-6 V.

The expression, written in the low-pass equivalent format, for the final output optical field is expressed by the following[7].

$$E_0(t) = \frac{E_i(t)}{2}\left[1 + e^{\frac{j\pi(V(t)+V_{bias})}{V_\pi}}\right] \tag{33}$$

$$= E_i cos\left[\frac{\pi}{2}\frac{(V(t) + V_{bias})}{V_\pi}\right] e^{-j\frac{\pi}{2}\frac{(V(t)+V_{bias})}{V_\pi}}$$

Where $E_{in}(t) = \sqrt{2P_o}e^{j\omega_c t}$ is the optical field at the input of the single-drive MZIM with angular a frequency, ωc, and average power P_o. The vestigial phase term $e^{-j\frac{\pi}{2}\frac{(V(t)+V_{bias})}{V_\pi}}$ is known as the chirp term and can be circumvented with the use of dual-drive MZIMs (two EOPMs). V_{bias} can be adjusted to generate different optical modulation formats: Optical Double Side Band (ODSB), Optical Single Side Band (OSSB and Optical Carrier Suppressed (OCS).

The chosen photonic modulation conducted in this dissertation is ODSB. A representation of an optical modulated LFM waveform is depicted in Figure 4.3.

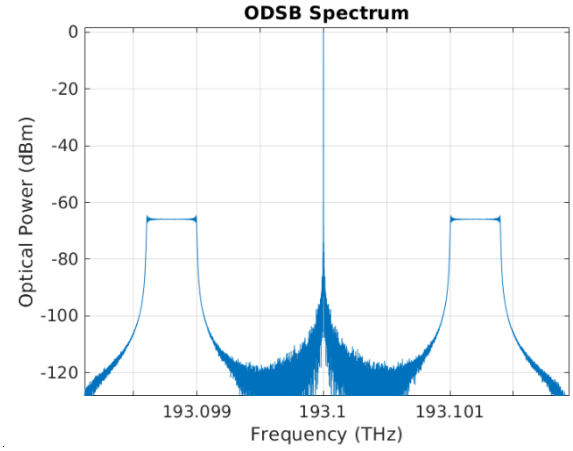

Figure 4.3 - ODSB radar signal centered at ITU reference optical frequency.

4.5. Optical to Electrical Conversion

The optical to electrical conversion is conducted by a photodetector. A photodetector converts light into electricity through the photoelectric effect.

The photocurrent originated by the photoelectric effect, I_P , is directly proportional to the incident optical power P_{in}. I_P is scaled by the responsivity, R, which is the ratio of the electrical output with the optical input.

$$I_P = R \times P_{in} \tag{34}$$

The responsivity of a positive-intrinsic-negative (PIN) photodetector (PD) is defined by

$$R = \frac{\eta \mathrm{q}}{\mathrm{h}f} \quad (A/W) \tag{35}$$

where η is the quantum efficiency, efficiency of photon to electron conversion, q is the electron charge, f is the frequency of the optical signal and h is the Planck´s constant.

In this dissertation, a PIN photodetector with responsivity of 1 A/W is assumed. The thermal noise of the receiver and the other disturbances are not considered.

4.6. Optical Heterodyning Method

Coherent heterodyning is a technique used to generate high frequency carrier signals by heterodyning two optical tones. Let E_1 be the first optical field tone defined by

$$E_1(t) = \sqrt{2P_1}e^{j(2\pi v_1 t + \theta_1(t))} \tag{36}$$

and E_2 the second tone defined by

$$E_2(t) = \sqrt{2P_2}e^{j(2\pi v_2 t + \theta_2(t))} \tag{37}$$

where P_1 and P_2 are the respective optical powers, v_1 and v_2 the optical frequencies, $\theta_1(t)$ and $\theta_2(t)$ the instantaneous phases [29].

Electrical signals are obtained by mixing the two optical tones upon photodetection by a photodiode (PD) with responsivity $\mathcal{R}$. The resultant photocurrent is given by

$$I(t) = \mathcal{R}|E_2(t) + E_1(t)|^2 \propto e^{j(2\pi(v_2 - v_1)t + \theta_2(t) - \theta_1(t))} + \text{other terms} \tag{38}$$

The mixing process leads to the generation of RF components at the sum and difference of the two input frequencies. Selection of the relevant harmonics (difference of the input frequencies) is conducted by means of an electric band-pass filter (BP).

This process can produce phase noise in the final RF carrier if the optical sources are not correlated, depicted in Figure 4.4. The requirement for correlated optical sources can be fulfilled with mode locked lasers (MLL) [30]. This process is conducted by optical filtering a pair of modes from the MLL spectrum and consequently heterodyning them. Although MLLs present stable phase locking, exterior factors such as laser operation temperature can introduce phase drifts between modes. The influence of partially incoherent heterodyning is one of the main performance evaluation points of the developed photonic radar simulation and is discussed in further detail in the following chapter.

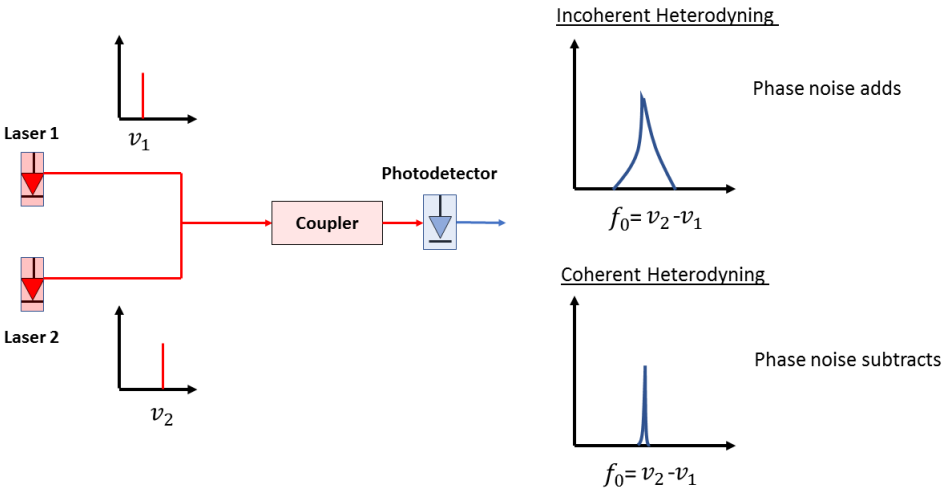

Figure 4.4 - Photonic MMWAVE generation. [31]

5 - Photonic FM-CW Radar Model

This chapter presents the simulation model of photonic supported radar. The first section covers the method used to generate the high frequency radar LFM waveform. Then, a complete radar system architecture based on [5] is explained. The final section presents the performance evaluation results.

5.1. Photonic Radar Uplink

A full photonic supported radar is based in upconverting and downconverting by means of optical heterodyning two or more optical tones.

The optical laser source considered is a MLL. In a MLL each mode operates with a fixed phase between it and the other modes. Such a laser is said to be 'mode-locked' or 'phase-locked'. The optical frequency spacing between the laser modes is constant. The generation of RF radar signals is carried out by first selecting the relevant modes from the MLL via a tunable optical filter (assumed as ideal filters) as represented in Figure 5.2 (A) and (B) where the optical frequency $\pm\Delta v/2$, is relative to a reference optical frequency of 0 Hz. The optical frequency spacing between the selected modes is Δv, it is selected to correspond the desired RF frequency (77 GHz). Once the relevant modes are selected, one optical mode is modulated with a MZIM. The driving voltage of the MZIM is the IF radar signal. The radar IF signal is a real signal localized at the IF frequency ($f_{I=}$*1 GHz*). The IF signal is obtained from the equivalent low pass as:

$$S_{IF}(t) = C_I cos(2\pi f_I t) - C_Q sin(2\pi f_I t) \quad (39)$$

$S_{IF}(t)$ is a real valued signal, whose spectrum is illustrated in Figure 5.1

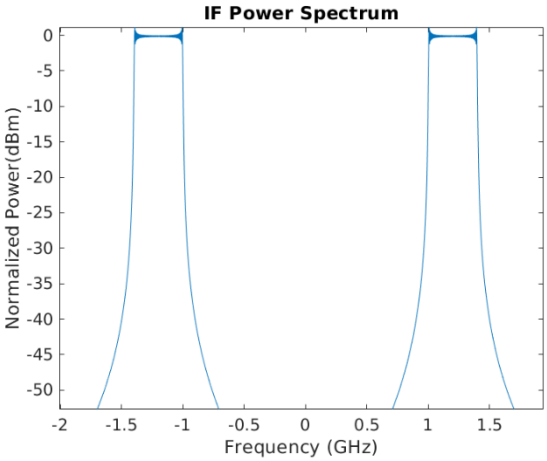

Figure 5.1 - IF radar LFM signal.

After modulation the modulated and unmodulated optical tones are coupled Figure 5.2 (C). After the optical coupler, a PD converts the signal from the optical to electrical domain. The resultant photodetected current signal contains higher and lower unwanted harmonics which are filtered out by an electrical bandpass filter, only the signal located at f_0 (77 GHz) is selected Figure 5.2 (D). The final RF frequency of the LFM waveform is located at f_0 which is defined by

$$f_0 = v_2 - v_1 = \Delta v \tag{40}$$

where v_1 is the optical frequency of optical mode which is not modulated, v_2 is the optical frequency optical mode which is modulated.

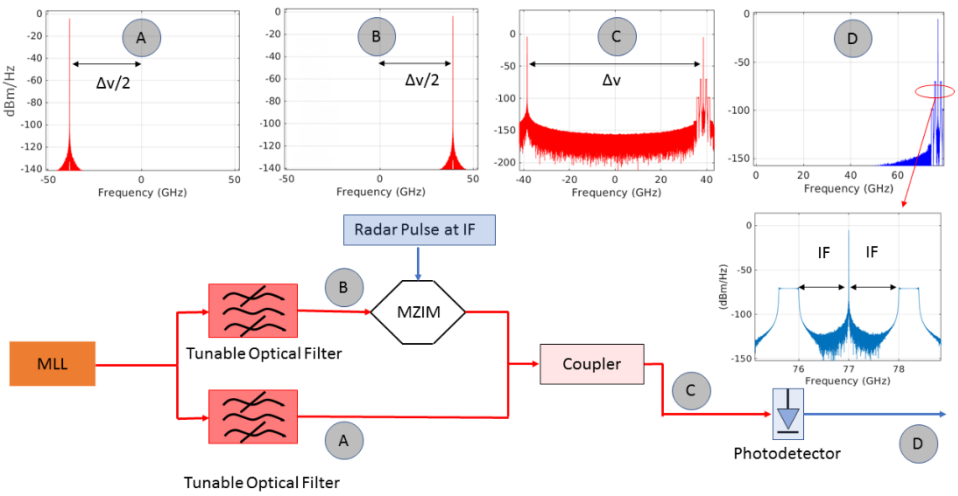

Figure 5.2 - Uplink photonic based radar. (A) Optical spectrum of MLL mode after optical filtering. (B) Optical spectrum of MLL after filter optical filtering. (C) Coupled MLL modes. (D) RF signal after optical heterodyning and electrical BP filtering. [5]

An approach based on the use of MLLs has been demonstrated experimentally[5]. Here, we have implemented a simulation model that quantifies how phase drifts between modes influence radar performance. This is a contribution to the field.

5.2. Photonic Radar Downlink

The downconverting process is carried out by driving a MZIM with the received radar echo. The optical input of the MZIM is a mode selected by a tunable optical filter, with an optical frequency of $\Delta v/2$, relative to a reference optical frequency of 0 Hz. After modulation, the modulated optical tone is heterodyned with the second optical tone with an optical frequency of $-\Delta v/2$ relative to the optical reference frequency. The downconverted electrical heterodyned signal is finally retrieved by band-pass filtering. By implementing upconversion/downconversion in the optical domain, the system impairments due the large phase noise of the high frequency LOs is avoided. A simple schematic of a full photonic based radar is illustrated in Figure 5.3.

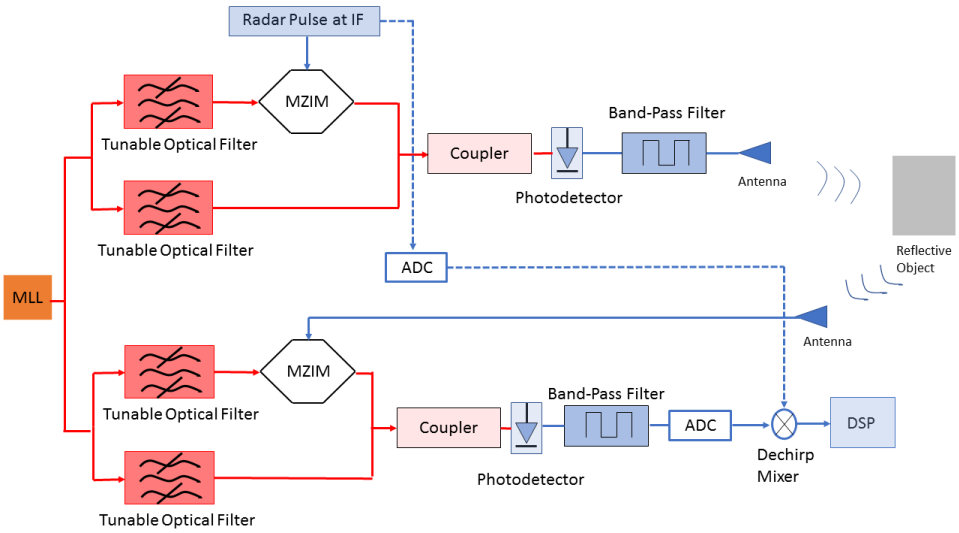

Figure 5.3 - Complete photonic radar system. [5]

The photonic radar simulation of this dissertation differs from figure 5.3, in that the downconversion process is treated as electrical. Imperfections of the electrical oscillators of the downlink were not accounted for, since the principal scope of this dissertation is the analysis of the photonic uplink.

A complete schematic of the simulation model implemented in this dissertation is illustrated in Figure 5.4.

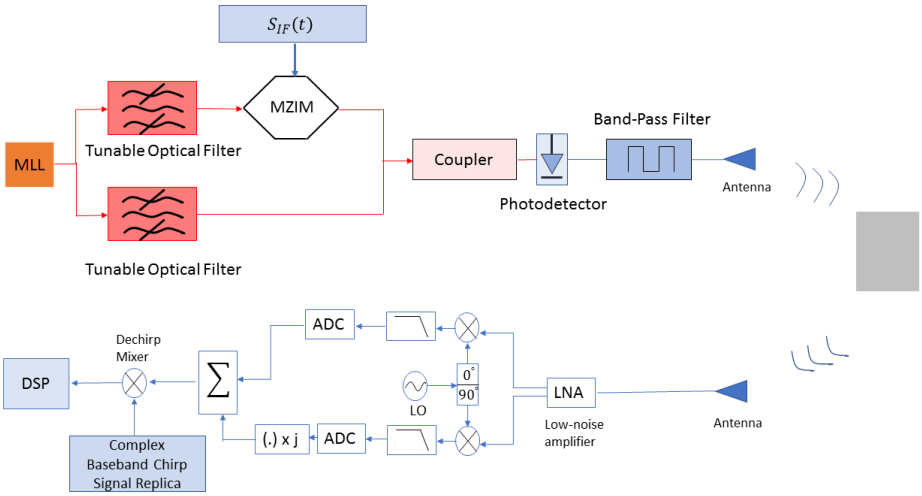

Figure 5.4 - Photonic radar simulation schematic.

Similarly, to the software defined signal generation of the system in section 3.2, the radar waveform is created digitally. The system then conducts the steps described in section 5.1. Once the echo is received an ideal IQ downconversion is conducted. The system finalizes operation by digitally mixing the received echo with a replica of the initially generated signal.

5.3. Radar Performance

5.3.1. System Parameters

System simulations were conducted with the parameters presented in Table 3. In the following simulations, some of these parameters will be changed and will be specified, the unspecified parameters remain the same.

	Parameter and description	**Value**	**Units**
Physical Parameters	c_o Light speed in vacuum	2.99792458×10^8	ms^{-1}
Radar Parameters	f_o Operation Frequency	77	GHz
	λ_o Operation Wavelength	$\frac{c_o}{f_o}$	m
	B LFM Bandwidth	400	MHz
	T LFM Time Period	6.8	μs
	$\propto$ Sweep Slope	$\frac{B}{T}$	s^{-2}

	T Sweep Interval	6.8	μs
	ΔR Range Resolution	0.375	m
	Δv Velocity Resolution	0.009975	ms^{-1}
	R_{max} Maximum Target Range	120	m
	V_{max} Maximum Target Speed	63.8	ms^{-1}
	P Mode Locked Laser Power	5	dBm
	MLL Linewidth	1	MHz
Other Parameters	f_s Sample Rate	$2 \times B$	Hz
	N Range FFT Length	2048	-
	L Velocity FFT Length	2048	-
	N_{sweep} Number of Sweeps	2048	-
	σ Target Mean RCS	0.25	m^2
	Receive Gain	60	dB
	Transmission Gain	60	dB
	Intermediate Frequency If	1	GHz

Table 3 – Photonic radar parameters

5.3.2. Impact of Phase Noise

The first simulation test was conducted to verify the effect of phase noise in the final range-speed response, depicted in Figure 5.5 and Figure 5.6. These figures present the electrical LFM signals Figure 5.5 a), Figure 5.6 a) and the corresponding range-speed responses Figure 5.5 b), Figure 5.6 b). The selected range and velocity input of the simulation model was 60 meters and 30 meters per second, respectively. Tests were conducted with an ideal MLL linewidth i.e. 1 Hz.

Phase noise of the optically generated signal arises when the laser modes are not completely coherent. Figure 5.5 depicts the ideal case when the MLL modes are ideally phased locked and with optical intensity noise not included. Figure 5.6 depicts the effects of incoherent heterodyning, in this case, the two decorrelated laser modes were heterodyned considering an intensity noise level of – 90 dBm.

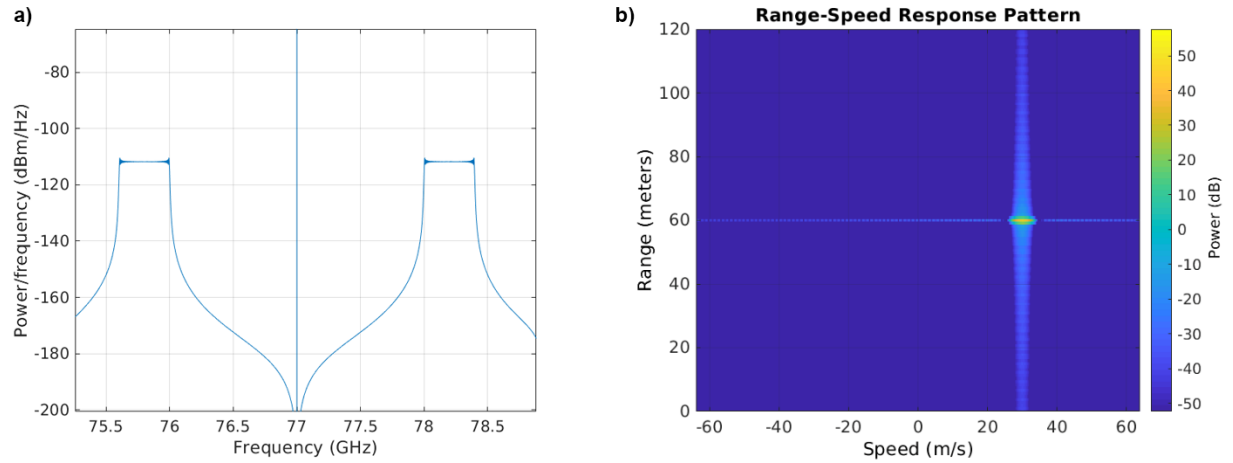

Figure 5.5 - Photonic radar system performance. a) Ideal Electrical radar signal. b) Range-speed response pattern without phase noise.

The effects of incoherent heterodyning of the MLL modes present in the electrical radar signal are depicted in Figure 5.6 a). Where the degradation of the modulated chirp signal and the formation of a noise skirt is visible.

Similarly, to the effects of phase noise in the electronic radar, phase noise creates false-positive targets along the range dimension, illustrated in Figure 5.6 b). With the first conducted tests it was possible to verify two main performance degradation aspects of photonic based radars. Namely, the level of intensity noise present in the MLL modes and the effects of incoherent heterodyning.

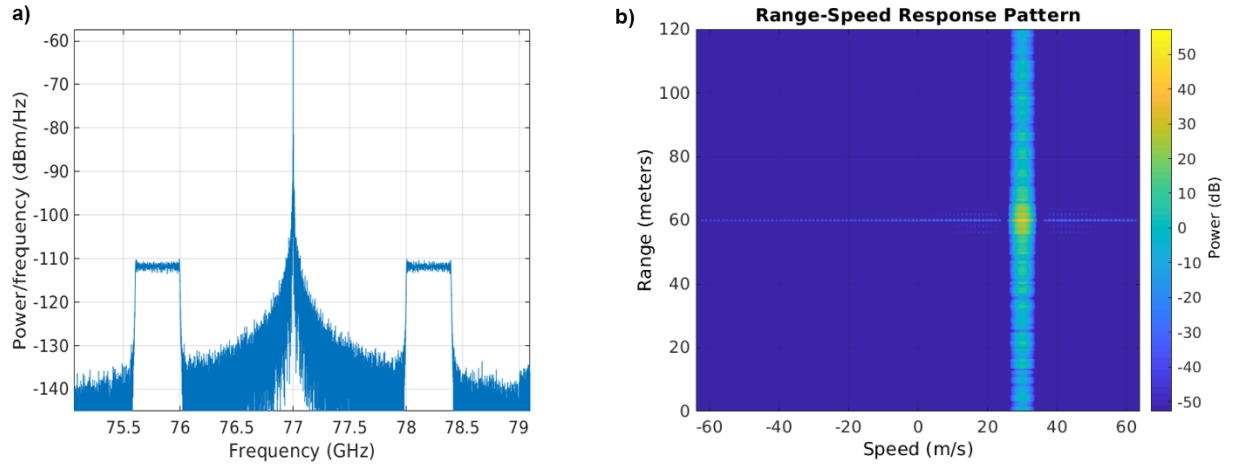

Figure 5.6 - Photonic radar system performance. a) Electrical noisy ODSB radar signal. b) Range-speed response pattern with phase noise

The next simulation test consisted in verifying range errors by varying the intensity noise level of the MLL in an interval of -100 dBm to -90 dBm. These tests were conducted to verify the influence of the MLL intensity noise in combination with three different MLL mode linewidths.

Figure 5.7 illustrates the evolution of range error, the difference between the estimated and real target range, in function of the MLL intensity noise for a MLL linewidth of 10 KHz. Three

different target locations were considered at a velocity of 5 m/s. When the MLL modes are completely correlated (coherently heterodyned) the system performs adequately for an intensity noise level of -100 dBm. It is visible in Figure 5.7 a) that targets, with the same velocity, that are further from the radar originate higher range errors. It is also visible that all the range error estimates are relatively high when the MLL mode intensity noise is -90 dBm.

Figure 5.7 b) illustrates the same target locations and velocity as Figure 5.7 a) but with decorrelated (incoherent heterodyned) MLL modes. The phase offset between the two MLL modes is 2 degrees. In comparison with Figure 5.7 a) the tests conducted in Figure 5.7 b) present higher range errors. Where the range errors for the three targets are similar before reaching the MLL intensity noise of - 98 dBm. Contrary to Figure 5.7 a), the tests conducted in Figure 5.7 b) demonstrate a larger error evolution for the target at 30 meters. This characteristic is caused by the reduced power of the echo signal from the target at 30 meters, the echo signal is masked by the noise skirt spectrum produced by incoherent heterodyning.

The overall evolution of the range errors presented in Figure 5.7 b) is larger than the range errors present in Figure 5.7 a). This is expected since the probability of error is higher in the presence of phase noise caused by incoherent heterodyning.

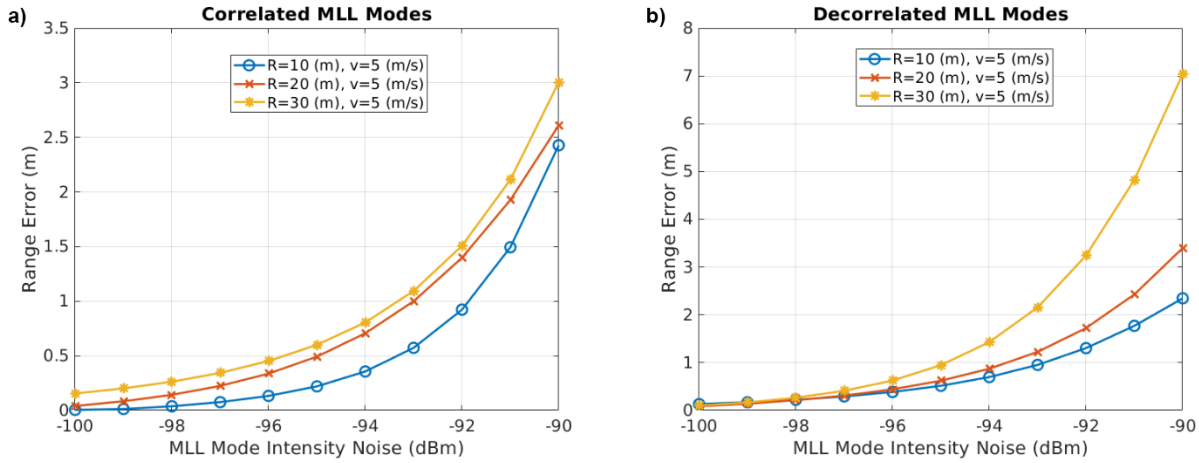

Figure 5.7 - Range error in function of MLL intensity noise. a) Correlated MLL modes. b) Decorrelated MLL modes.

Figure 5.8 depicts the test results conducted with linewidths of 1MHz and 10 MHz where the MLL modes were incoherent heterodyned with a phase offset of 2 degrees. These linewidths were selected as a term of comparison for the tests conducted in Figure 5.7 b). By comparing Figure 5.7 b) with Figure 5.8 a) b) it is notable that the system performance is highly impaired for larger MLL linewidths. This fact combined with a phase offset, between the MLL modes, in the heterodyning process causes relatively higher measurement accuracy errors. The errors present in the range estimations when the MLL linewidth is 10 MHz, Figure 5.8 b), are notably high. Therefore, it is

concluded that the viability of the system with decorrelated MLL mode linewidths superior to 1 MHz is reduced. More in-depth system performance tests on the effect of MLL mode linewidths are presented in the following subsection.

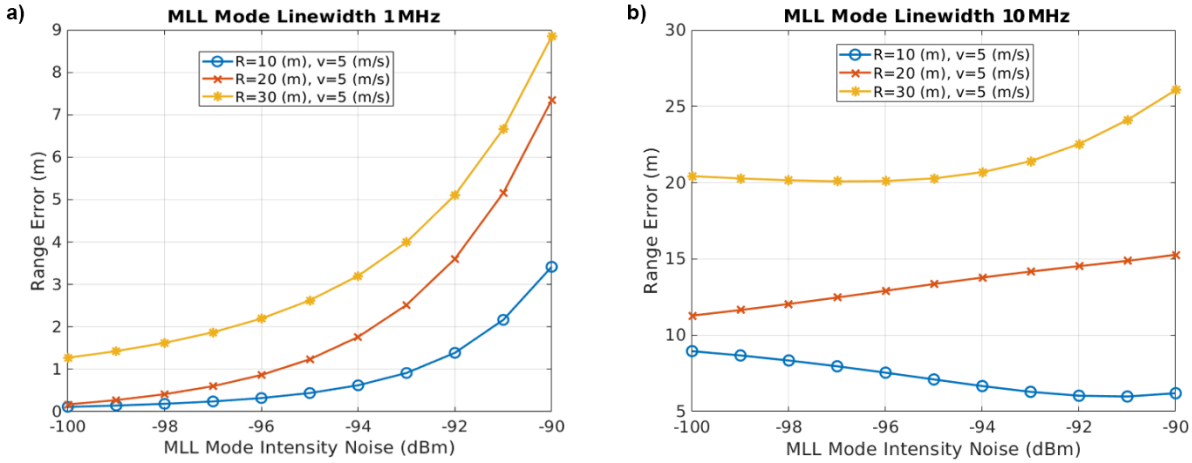

Figure 5.8 - Range Error in function of MLL intensity noise. a) Decorrelated, MLL linewidth, 1 MHz. b) Decorrelated, MLL linewidth, 10 MHz.

5.3.3. Effect of MLL Mode Linewidth

The effect of the MLL mode linewidths on system performance is illustrated in Figure 5.9. Where the MLL mode linewidths were incremented in an interval of 1 Hz to 10 MHz. The MLL modes are considered to be decorrelated. Range errors were then calculated in function of the MLL mode linewidths in the absence of intensity noise. Figure 5.9 a) demonstrates the variation of range errors with three targets with the same velocity. It is visible that the target at 30 meters is greatly affected from the effect of incrementing the MLL linewidths. It can also be noted that the system provides lower range errors for the target at 30 meters when the MLL linewidths are less than 1MHz. Targets at a range of 10 and 20 meters present higher errors when the linewidths are higher than 2 MHz. Figure 5.9 b) illustrates the range error for targets at the same location (10 meters) with different velocities. Targets moving with higher velocities present partially higher range errors which is visible in Figure 5.9 b). The system performs with minimal range errors for all velocities when the MLL linewidths are less than 1MHz.

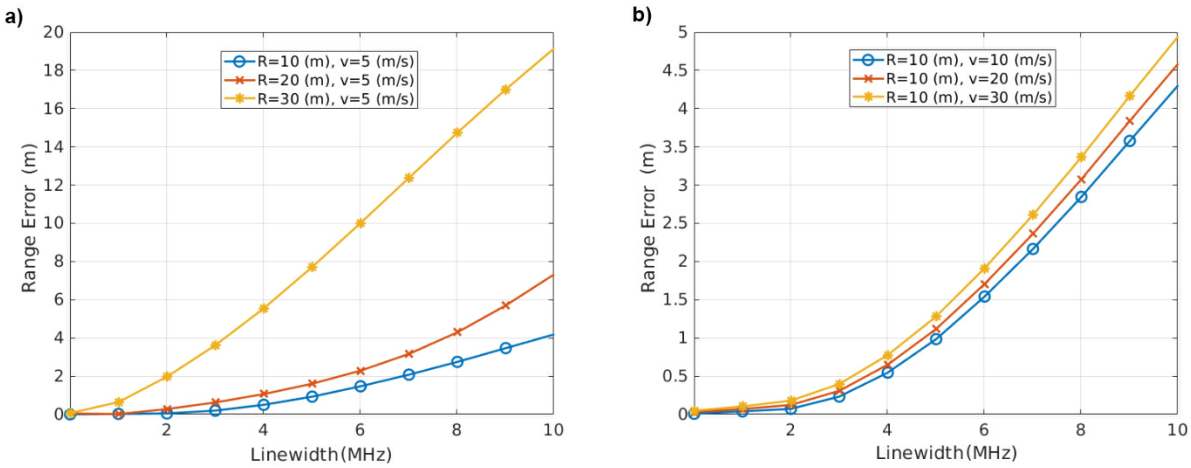

Figure 5.9 - Range error in function of MLL linewidths. a) Equal target velocities. b) Equal target ranges.

5.3.4. System Figure of Merit

The last performance evaluation tests were performed to assess the relationship between the OSNR of the MLL modes and SNR of the range dechirped signal. A Figure of Merit was defined by the following equation

$$Figure\ of\ Merit = \frac{Dechirped\ Signal\ SNR}{MLL\ Mode\ OSNR} \tag{41}$$

Tests were selected to give an overall overview of the system performance. Figure 5.10 illustrates the conducted tests.

The MLL mode OSNR was incremented by varying the intensity noise in an interval of -90 to -160 dBm. Figure 5.10 a) illustrates the test results for MLL linewidths of 10 KHz. The target was located at a range of 10 meters and had a velocity of 5 m/s. In Figure 5.10 a) it is notable that the decorrelated system performance is limited to a maximum dechirp signal SNR of 34 dB, this demonstrates that the system will reach a lower performance asymptote when decorrelation between MLL modes occurs. The difference between the performance asymptote of the correlated and decorrelated MLL modes is 16 dB. This difference is proportional to the MLL linewidths. Figure 5.10 b) illustrates a larger difference in performance when the MLL mode linewidths are 1 MHz.

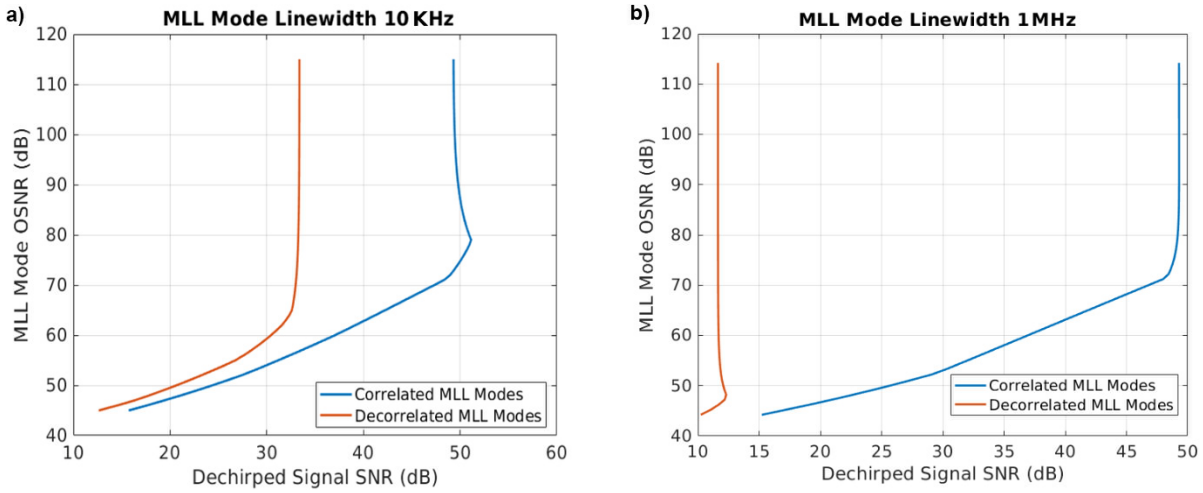

Figure 5.10 - MLL mode OSNR in function of dechirped signal SNR. a) MLL mode linewidths 10 KHz. b) MLL mode linewidths 1 MHz.

The calculated overall figure of merit of the system when the linewidths are 10KHz, for decorrelated MLL modes, is equal to 0.3878 and the figure of merit for correlated modes is equal to 0.5446. When the MLL mode linewidths are equal to 1 MHz the system presents a figure of merit of 0.1463 and 0.5442 for decorrelated and correlated MLL modes, respectively.

To finalize the performance analysis of the photonic supported radar, range errors were calculated and plotted against the dechirped signal SNR. Figure 5.11 a) depicts this relationship for correlated modes with a linewidth of 10 KHz. Figure 5.11 b) depicts the same relationship for decorrelated modes with the same MLL mode linewidth as Figure 5.11 a). Figure 5.11 a) b) present minimum range errors when the dechirped signal SNR is superior to 32 dB. By referring to Figure 5.10 a) it is possible to verify the corresponding MLL mode OSNR to which the system performs with minimized error. A dechirped signal SNR of 32 dB corresponds to a MLL mode OSNR of 55 dB for correlated modes and 60 dB for decorrelated modes. Which means, that to have the same performance as the correlated system, the MLL mode OSNR of the decorrelated system must be larger by 5dB.

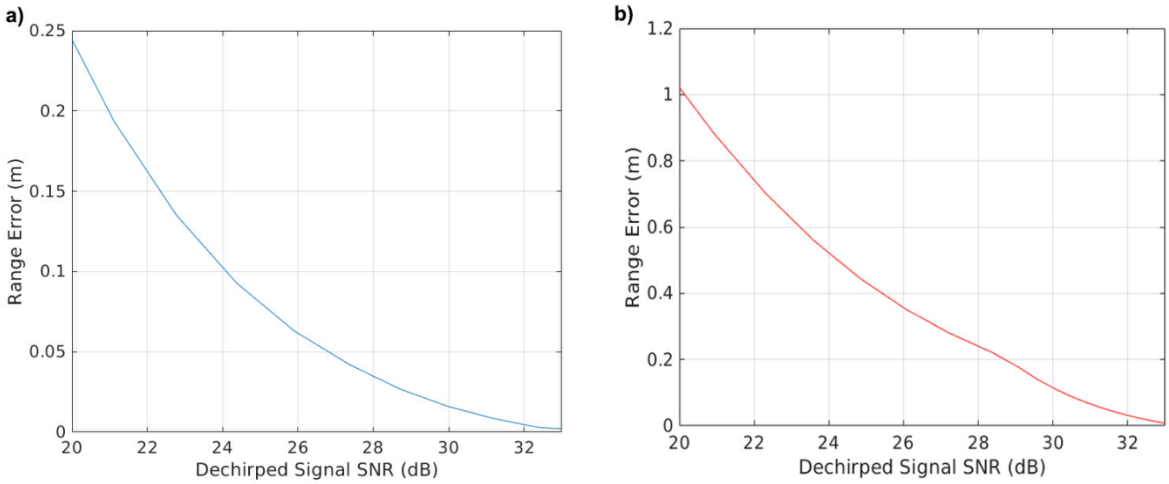

Figure 5.11 - Range error in function of Dechirped Signal SNR. a) MLL mode linewidth 10 kHz correlated modes. b) MLL mode linewidth 10 kHz decorrelated modes.

The conducted performance evaluation tests, for the parameters specified in table 3, lead to the following conclusions. MLL mode OSNRs should have a value superior to 60 dB, MLL mode linewidths should be less than to 1 MHz and MLL mode correlation in the optical heterodyning method should be guaranteed.

6 - Conclusions

In this chapter, the conclusions of this work are discussed in the first section. The second section presents suggestions of future work.

6.1. Conclusions and Contributions

In this dissertation, two FM-CW radar systems models were implemented using Matlab: a fully electronic radar system and a photonic supported radar system. The implemented software models were used to assess system performance.

The electronic system model was used to study the importance of pulse compression on FM-CW radar system performance. The effect of the local oscillator phase noise on range estimations was analyzed by fitting the simulated local oscillator phase noise with the phase noise profile of a USRP. It was shown that bandwidth and phase noise are critical parameters of electronic FM-CW radars. High performance FM-CW radars should have high bandwidth and low oscillator phase noise. These two objectives can be fulfilled by photonic based radars.

Key photonic technologies necessary for the implementation of a photonic supported radar were studied. Using the models of the photonic components and the model of the electronic radar the next step was the implementation of a photonic supported radar model.

Performance evaluation of the photonic radar system simulation model highlighted several system parameters which impair system performance. Namely, low MLL mode OSNR, large linewidths of the optical tones and the decorrelation between the optical tones. It was demonstrated that the system OSNR must considerably high (> 60 dB). It was also demonstrated that phase offsets present between the two optical tones which are heterodyned caused considerably large range errors. This fact combined with large tone linewidths was verified to be the most relevant performance limiting factor.

The objectives of the dissertation were fulfilled. The major contribution of this work is the implemented simulation model that will be useful in the design and evaluation of photonic supported radars.

6.2. Future Work

In this section, suggestions on future work are presented:

1. A complete (Uplink/Downlink) photonic radar system should be simulated.
2. The effect of optical fiber transmission should be included in the model.
3. The impact and design considerations of using the same MLL for up- and downconversion should be assessed.

4. The value of the intermediate frequency for the electrical radar signal and its impact on the performance of the system should be verified.
5. The delay introduced by the MZIM and other optical components should be included in the model and the effects on system performance should be studied as well as compensation schemes.
6. System performance degradation of non-ideal optical filters should be verified.
7. Development of an intuitive Graphical User's Interface with Matlab that facilitates the input of various system parameters.
8. Computational optimization of the developed Matlab methods.
9. Digital radar processing with the CFAR algorithm.

References

[1] S. Mark A.Richards, James A, *Principles of Modern Radar:Basic Principles*. 2015.

[2] J. Hasch, E. Topak, R. Schnabel, T. Zwick, R. Weigel, and C. Waldschmidt, "Millimeter-wave technology for automotive radar sensors in the 77 GHz frequency band," *IEEE Trans. Microw. Theory Tech.*, vol. 60, no. 3 PART 2, pp. 845–860, 2012.

[3] Q. Wu, W. Tao, Y. D. Zhang, and M. G. Amin, "Radar-based fall detection based on Doppler time–frequency signatures for assisted living," *IET Radar, Sonar Navig.*, vol. 9, no. 2, pp. 164–172, 2015.

[4] M. He, Y. Nian, and Y. Gong, "Novel signal processing method for vital sign monitoring using FMCW radar," *Biomed. Signal Process. Control*, vol. 33, pp. 335–345, 2017.

[5] P. Ghelfi *et al.*, "A fully photonics-based coherent radar system," *Nature*, vol. 507, no. 7492, pp. 341–345, 2014.

[6] F. Scotti *et al.*, "In-field experiments of the first photonics-based software-defined coherent radar," *J. Light. Technol.*, vol. 32, no. 20, pp. 3365–3372, 2014.

[7] T. Kawanishi, A. Kanno, N. Yamamoto, N. Yonemoto, N. Shibagaki, and K. I. Kashima, "Optical fiber network-connected distributed mm-wave radar system," *Summer Top. Meet. Ser. SUM 2017*, pp. 197–198, 2017.

[8] S. Futatsumori, K. Morioka, A. Kohmura, K. Okada, and N. Yonemoto, "Design and field feasibility evaluation of distributed-type 96 GHz FMCW millimeter-wave radar based on radio-over-fiber and optical frequency multiplier," *J. Light. Technol.*, vol. 34, no. 20, pp. 4835–4843, 2016.

[9] Bassem R. Mahafza, *Radar Systems Analysis and Design Using MATLAB*. 2013.

[10] P. Bezousek, M. Hajek, and M. Pola, "Effects of signal distortion in a FMCW radar on range resolution," *Proc. 15th Conf. Microw. Tech. Com. 2010*, no. 1, pp. 113–116, 2010.

[11] P. D. L. Beasley, "The influence of transmitter phase noise on FMCW radar performance," *Proc. 3rd Eur. Radar Conf. EuRAD 2006*, no. September, pp. 331–334, 2007.

[12] J. R. Klauder, A. C. Price, S. Darlington, and W. J. Albersheim, "The Theory and Design of Chirp Radars," *Bell System Technical Journal*, vol. 39, no. 4. pp. 745–808, 1960.

[13] D. Barton, *System Analysis and Modeling*. Artech House, 2005.

[14] M. . Richards, "Fundamentals of Radar Signal Processing," *IEEE Signal Processing Magazine*. 2009.

[15] M. Skolnikl, *Radar Handbook 3rd*. 2008.

[16] E. Rubiola, "Phase Noise and Frequency Stability in Oscillators (The Cambridge RF and

Microwave Engineering Series)," 2008.

[17] N. J. Kasdin, "Discrete simulation of colored noise and stochastic processes and 1/f/sup α/ power law noise generation," *Proc. IEEE*, vol. 83, no. 5, pp. 802–827, 1995.

[18] H. Schmid, "IME Report 01 / 2009 : How to use the FFT for signal and noise simulations and measurements," pp. 1–8, 2009.

[19] L. Pursell and S. . Trimble, "Gram-Schmidt Orthogonalization by Gauss Elimination," *Am. Math. Mon.*, vol. 98, no. 6, pp. 544–549, 1991.

[20] J. A. Scheer, "Coherent radar system performance estimation," *IEEE Int. Conf. Radar*, pp. 125–128, 1990.

[21] R. H. Walden, "Analog-to-digital conversion in the early twenty-first century," *Wiley Encycl. Comput. Sci. Eng.*, pp. 126–138, 2008.

[22] J. Capmany and D. Novak, "Microwave photonics combines two worlds," *Nat. Photonics*, vol. 1, no. 6, pp. 319–330, 2007.

[23] L. Goldberg, R. D. Esman, and K. . Williams, "Generation and control of microwave signals by optical techniques," *IEE Proc. J Optoelectron.*, vol. 139, no. 4, pp. 288–295, 1992.

[24] J. Chou, Y. Han, and B. Jalali, "Adaptive RF-photonic arbitrary waveform generator," *IEEE Photonics Technol. Lett.*, vol. 15, no. 4, pp. 581–583, 2003.

[25] P. Ghelfi, F. Laghezza, F. Scotti, G. Serafino, S. Pinna, and A. Bogoni, "Photonic generation and independent steering of multiple RF signals for software defined radars," *Opt. Express*, vol. 21, no. 19, p. 22905, 2013.

[26] C. Browning, E. P. Martin, A. Farhang, and L. P. Barry, "60 GHz 5G Radio-Over-Fiber Using UF-OFDM with Optical Heterodyning," *IEEE Photonics Technol. Lett.*, vol. 29, no. 23, pp. 2059–2062, 2017.

[27] M. P. Thakur, M. C. R. Medeiros, P. Laurencio, and J. E. Mitchell, "Optical frequency tripling with improved suppression and sideband selection," *Opt. Express*, vol. 19, no. 26, pp. B459–B470, 2011.

[28] G. P. Agrawal, *Fiber-Optic Communication Systems*, vol. 6. New York, 2002.

[29] J. J. O'Reilly, P. M. Lane, R. Heidemann, and R. Hofstetter, "Optical generation of very narrow linewidth millimetre wave signals," *Electron. Lett.*, vol. 28, no. 25, pp. 2309–2311, 1992.

[30] G. Serafino *et al.*, "Stable optically generated RF signals from a fibre mode-locked laser," *2010 23rd Annu. Meet. IEEE Photonics Soc. PHOTINICS 2010*, no. 4, pp. 193–194, 2010.

[31] M. C. R. Medeiros, P. Almeida, B. M. Oliveira, P. Laurencio, and P. M. Monteiro, "Fiber wireless-optical transceiver architectures for 60 GHz LANs," *Int. Conf. Transparent Opt. Networks*, pp. 1–4, 2017.